

Principles of mRNA control by human PUM proteins elucidated from multi-modal experiments and integrative data analysis

Michael B. Wolfe^a, Trista L. Schagat^b, Michelle T. Paulsen^c, Brian Magnuson^{d,e}, Mats Ljungman^{c,f}, Daeyoon Park^g, Chi Zhang^h, Zachary T. Campbell^h, Aaron C. Goldstrohm^g, Peter L. Freddolino^a

^a*Department of Biological Chemistry and Department of Computational Medicine & Bioinformatics, University of Michigan, Room 5301 MSRB III, 1150 W. Medical Center Dr., Ann Arbor, MI 48109, USA*

^b*Promega Corporation, 2800 Woods Hollow Rd #5399, Fitchburg, WI, 53711, USA*

^c*Department of Radiation Oncology, University of Michigan, Ann Arbor, MI 48109, United States*

^d*Department of Biostatistics, School of Public Health, University of Michigan, Ann Arbor, MI 48109, United States*

^e*Rogel Cancer Center, University of Michigan, Ann Arbor, MI 48109, United States*

^f*Department of Environmental Health Sciences, University of Michigan, Ann Arbor, MI 48109, United States*

^g*Department of Biochemistry, Molecular Biology and Biophysics, University of Minnesota, Room 6-155, Jackson Hall, 1214A, 321 Church Street SE, Minneapolis, MN, 55455, USA*

^h*Department of Biological Sciences, University of Texas at Dallas, Richardson, TX 75080, United States*

Abstract

The human PUF-family proteins, PUM1 and PUM2, post-transcriptionally regulate gene expression by binding to a PUM recognition element (PRE) in the 3' UTR of target mRNAs. Hundreds of PUM1/2 targets have been identified from changes in steady state RNA levels; however, prior studies could not differentiate between the contributions of changes in transcription and RNA decay rates. We applied metabolic labeling to measure changes in RNA turnover in response to depletion of PUM1/2, showing that human PUM proteins regulate expression almost exclusively by changing RNA stability. We also applied an *in vitro* selection workflow to precisely identify the binding preferences of PUM1 and PUM2. By integrating our results with prior knowledge, we developed a 'rulebook' of key contextual features that differentiate functional vs. non-functional PREs, allowing us to train machine learning models that accurately predict the functional regulation of RNA targets by the human PUM proteins.

Keywords: RNA decay, Pumilio, Machine Learning

1. Introduction

The control of gene expression at the post-transcriptional level is critical for diverse biological processes including proper organismal development in multicellular organisms. Many regulators, including RNA-binding proteins (RBPs), act to control the stability of target mRNA transcripts through the recognition of key sequence elements in the 3' UTRs of mRNAs [1, 2]. A recent survey of all known human RBPs indicated that a substantial fraction of human RBPs bind to mRNAs, however, for any given RBP, the binding specificity, set of mRNA targets, and functional role for the RBP at each target still remains poorly understood [3].

The PUF (Pumilio and FBF [fem-3 binding factor]) family of proteins represent one of the most well-studied classes of RBPs [1, 4, 5]. PUF proteins possess a shared C-terminal Pum homology

Email addresses: agoldstr@umn.edu (Aaron C. Goldstrohm), petefred@umich.edu (Peter L. Freddolino)

11 domain (PUM-HD). Structurally, the human PUM-HD consists of 8 helical repeats containing
12 specific amino acids that both intercalate and form hydrogen bonds and van der Waals contacts
13 with target RNA, resulting in exquisite specificity for a UGUANAUUA consensus sequence motif or
14 PUM Recognition Element (PRE) [6, 7]. Recognition by the PUM-HD is modular and specificity
15 for a given base can be changed through mutation of a set of three key amino acids in a single
16 repeat [7, 8]. Furthermore, the sequence specificity by PUM-HD across species can be predicted
17 from the identity of these three key amino acids across the helical repeats in any given PUM-HD
18 [9]. Thus, there are slight differences in the exact set of sequences recognized by the PUM-HD
19 of different PUF family members and, in addition, interactions with protein partners can alter
20 sequence preference [10–12].

21 Functionally, the PUF family of proteins have been implicated in post-transcriptional regu-
22 lation underlying control of developmental processes [1]. One of the founding members of the
23 family, *Drosophila* Pum, together with the Nos protein, is needed for correct body patterning in
24 the developing fly embryo [13, 14]. Patterning is accomplished by location-specific repression of
25 the *hunchback* mRNA through sequence-specific recognition of a nanos response element (NRE)
26 in the *hunchback* 3' UTR [15]. In humans, there are two members of the PUF family, PUM1 and
27 PUM2, which share 75% overall sequence identity with 91% sequence identity in the PUM-HD.
28 In addition, human PUM1 and PUM2 share 78% and 79% sequence identity in the PUM-HD to
29 DmPum, respectively [5, 16]. Human PUM1 and PUM2 are expressed across tissues and their ex-
30 pression is highly overlapping [5, 16] suggesting that they likely act redundantly. Mammalian PUM
31 proteins have been implicated in spermatogenesis [17, 18], neuronal development and function[19–
32 24], immune function [25, 26], and cancer [27–30]. PUM1 missense and deletion mutants lead to
33 adult-onset ataxia (Pumilio1-related cerebellar ataxia, PRCA) and loss of one copy leads to de-
34 velopmental delay and seizures (Pumilio1-associated developmental disability, ataxia, and seizure;
35 PADDAS) [31]. Yet, the targets responsible for these biological outcomes are largely opaque.

36 Targeted experiments have indicated that human PUM1 and PUM2 are capable of repressing
37 expression of a luciferase reporter through recognition of PREs in the reporter gene's 3' UTR,
38 likely through recruitment of the CCR4-NOT complex and subsequent degradation of the mRNA
39 target [32]. Additionally, similar assays have shown that repression by the human PUM2 PUM-
40 HD alone—that is lacking the N-terminal domains of PUM2—requires the polyA binding protein
41 PABPC1, suggesting that the human PUMs could accelerate mRNA degradation by inhibiting
42 translation [33]. However, PUM-mediated repression is not the only type of gene regulation by
43 human Pumilio proteins. Recently, expression of a key regulator of hematopoietic stem cell dif-
44 ferentiation, FOXP1, was shown to be enhanced by human PUM1/2 binding to the 3' UTR [29].
45 Furthermore, measurements of changes in global steady-state RNA abundance between wild-type
46 (WT) and PUM1/2 knockdown conditions have identified hundreds of RNAs that either increase
47 or decrease in abundance upon PUM1/2 knockdown [34]. Follow-up experiments have confirmed
48 activation of key targets by human PUMs through the use of a reporter gene-target 3' UTR fusion
49 construct [34], indicating that human PUMs directly activate some mRNA targets. However, the
50 mechanism of PUM-mediated activation remains to be elucidated.

51 High-throughput measurements of PUM1 and PUM2 binding sites *in vivo* have confirmed high
52 specificity for a PRE and have identified a diverse set of PUM targets in human cell lines, including
53 those involved in regulating neuronal function and signaling cascades [35–38]. Thus, sequence-
54 specific recognition of the PRE is an important aspect of target recognition for the PUM proteins.
55 However, key questions about PUM-mediated gene regulation remain. There are on the order of
56 10,000 PRE sites across the full set of annotated human 3' UTRs, but only ~1000 genes change in
57 steady state RNA levels under PUM1/2 knockdown [34]. Additionally, models using a simple count
58 of PREs in the 3' UTR of a transcript do not completely capture the complexity of PUM-mediated

59 gene regulation [34]. The identification of additional sequence features that discriminate functional
60 PREs from apparently non-functional PREs will improve the understanding of PUM-mediated
61 gene regulation. Furthermore, as the measurement of steady-state RNA levels do not allow for
62 differentiation between the individual contributions of transcription rates and RNA stability, we
63 instead set out to directly measure changes in RNA stability under PUM1/2 knockdown condi-
64 tions. Through the use of high-throughput sequencing methodologies, we demonstrate that human
65 PUM1/2 modulate the abundance of mRNA targets primarily through controlling mRNA stability
66 and not transcription rates. We demonstrate, through high-throughput *in vitro* binding assays,
67 that PUM1 and PUM2 PUM-HDs have highly similar preferences for the same sets of sequences.
68 Consistent with prior reports, we find that PUM1/2 control the mRNA stability of transcripts
69 involved in signaling pathways, neuronal development, and transcriptional control. In addition, we
70 identify a key set of contextual features around PREs that contribute meaningful information in
71 predicting PUM-mediated regulation including proximity to the 3' end of a transcript and the AU
72 content around PRE sites. Taken together, our study illuminates key contributors to determining
73 functional PRE sites and represents a rich resource for interrogating the control of mRNA stability
74 by the PUM RBPs.

75 2. Results

76 2.1. Bru-seq and BruChase-seq reveal PUM-mediated effects on mRNA stability

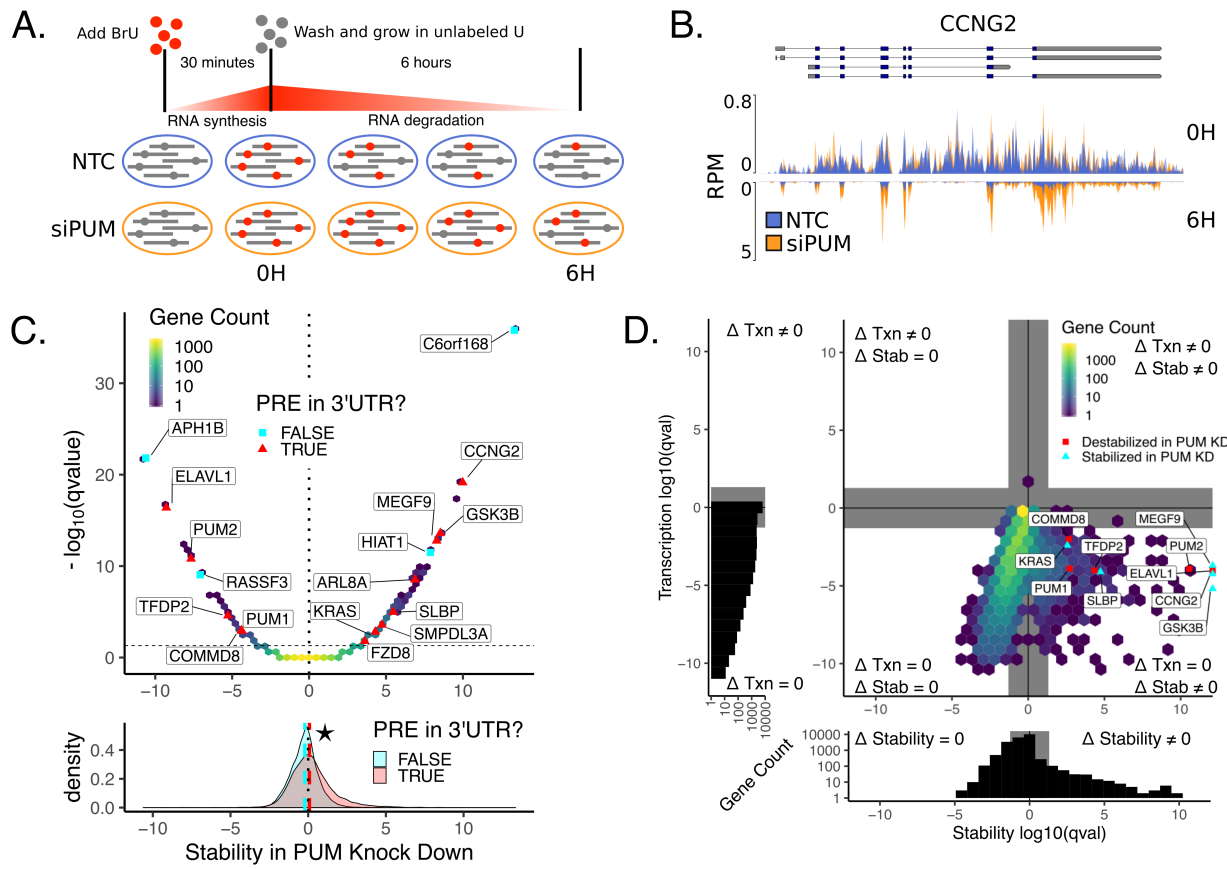
77 In order to measure the effect of the human PUM1 and PUM2 proteins on mRNA stability at a
78 transcriptome-wide scale, we employed the Bru-seq and BruChase-seq methodology [39]. In brief,
79 Bru-seq and BruChase-seq involve the metabolic labeling of RNA using 5-bromouridine (BrU),
80 which is readily taken up by the cells and incorporated into the nascent NTP pool [40]. After
81 incubation with BrU over a short time period, newly synthesized and labeled RNAs are selectively
82 pulled out of isolated total RNA using an anti-BrdU antibody and sequenced. Labeled RNA abun-
83 dance is then tracked over time by continuing to grow the cells in the absence of BrU and isolating
84 BrU-labeled RNA at additional time points. To distinguish relative changes in transcription rates
85 from relative changes in RNA stability between WT and PUM1/2 knockdown cells, we chose two
86 time points: (1) a zero hour time point taken at the transition to unlabeled media after 30 minutes
87 of incubation in BrU-containing media and (2) at six hours, a time point chosen to coincide with the
88 average mRNA half-life in cultured mammalian cells [41–43]. To determine the impact of PUM1/2
89 on relative RNA abundances, the experiment was performed in the presence of a mix of siRNAs
90 targeting both *PUM1* and *PUM2* mRNAs (siPUM) or in the presence of scrambled non-targeting
91 control siRNAs (NTC), as previously established [32, 34](Figure 1A). Cells were treated with siR-
92 NAs for 48 hours before BrU labeling, identically to the method used in Bohn et al. [34], to allow
93 for PUM depletion prior to labeling. Overall, four biological replicate samples were collected for
94 each time point and RNAi condition resulting in a total of 16 samples and above the minimum
95 recommendations for replicates suggested by the ENCODE consortium for RNA-seq and ChIP-seq
96 experiments [44, 45]. HEK293 cells were chosen for this study as they express both PUM1 and
97 PUM2, have been previously used to analyze PUM activity [32, 34], support efficient BrU-labeling
98 [46], and support RNA interference [47]. As we have previously demonstrated [32, 34], knockdown
99 of both PUM1 and PUM2 is necessary to alleviate PUM repression of PRE-containing mRNAs. It
100 is important to note that the use of two time points does not allow for determination of full decay
101 rate constants for each transcript, but it does allow for measurements of relative changes in mRNA
102 stability between the two conditions [48].

103 Clear changes in RNA abundance can be seen between time points and conditions at the gene
104 level. Consider the Cyclin G2 (CCNG2) mRNA which encodes a cyclin involved in the cell cycle,

105 contains 2 PREs in its 3' UTR, and was among the most dramatically affected mRNAs (Figure
106 1B). At the 0 hr time point, read coverage resulting from recent transcription for four distinct
107 replicates in each condition can be seen (Read coverage includes immature RNAs that still contain
108 introns) (Figure 1B top). At the six hour time point, only mature RNA remains, with read coverage
109 primarily observed at exons and no longer prevalent in the intronic regions (Figure 1B bottom).
110 Here, silencing of both PUM1 and PUM2 clearly increases RNA abundance relative to the non-
111 targeting control at the 6 hr time point, but does not appear to impact transcription as seen at the
112 0 hr time point.

113 To quantify the effect of silencing PUM1 and PUM2 on changes in relative labeled RNA abun-
114 dance between the 0 and 6 hour time points, we used DEseq2 [49] to model the count of reads
115 observed from each gene using a generalized linear model that considers the effects of time, condi-
116 tion, and the interaction between time and condition (see Methods for details). We interpret the
117 term associated with the interaction between condition and time to be the PUM-mediated effect
118 on stability—where a positive value indicates that an RNA was stabilized in the PUM knockdown
119 condition and a negative value indicates that an RNA was de-stabilized in the PUM knockdown
120 condition. Likewise, we interpret the condition term as the PUM-mediated effect on transcription
121 rates, thus, we are able to separate the impacts of transcription from RNA stability using our exper-
122 imental procedure and statistical methodology. We find that hundreds of genes show altered RNA
123 stability under PUM knockdown conditions. Figure 1C displays an overview of PUM-mediated ef-
124 fects on stability as a volcano plot, with 12,165 genes represented in a two-dimensional histogram.
125 Using an FDR-corrected p-value threshold of 0.05 and a fold-change cutoff of $\log_2(1.75)$ (see Meth-
126 ods), we found 44 genes were statistically significantly de-stabilized (56 with no fold-change cutoff)
127 and 200 genes were statistically significantly stabilized in the PUM knockdown condition (252 with
128 no fold-change cutoff). Of these genes, 30 were also identified as having lower abundance under
129 PUM knockdown in the Bohn et al. [34] RNA-seq data set (37 with no fold-change cutoff). Like-
130 wise, 95 were also identified as having higher abundance under PUM knockdown in the Bohn et al.
131 [34] RNA-seq data set (106 with no fold-change cutoff). As expected, in our data both *PUM1*
132 and *PUM2* were substantially destabilized in the PUM knockdown condition relative to the WT
133 condition indicating that the siRNAs were successful in disrupting PUM1/2 expression and that
134 our methodology is capable of detecting known changes in RNA stability. Additionally, we found
135 that genes with a PRE in their 3' UTR were, on average, more stabilized in the PUM knockdown
136 condition than those without a PRE in their 3' UTR (Figure 1C bottom). Taken together, this
137 suggests that PUM1/2 are selectively modulating the RNA stability of target transcripts.

138 To further examine the effects of PUM knockdown on both transcription and stability, we tested
139 for statistically significant changes under a null model centered around a \log_2 fold change of 0 for
140 both the condition term (transcription) and the interaction between condition and time (stability).
141 In addition, for each term, we also tested for a statistically significant lack of change by considering
142 a null model centered around the boundary of a defined region of practical equivalence spanning
143 from $-\log_2(1.75)$ to $\log_2(1.75)$ (see Methods for details); such a test is important because failure
144 to reject the null hypothesis cannot, by itself, be taken as evidence favoring the alternative. In
145 total, four statistical tests were run for each gene: a test for change and a test for no change for
146 both transcription and stability. For each axis, the smaller of the two FDR-corrected p-values (i.e.
147 test for change vs. test for no change) was chosen as the coordinate for that term, which enabled
148 classification of each gene into one of four quadrants: 1. Genes that change in both stability and
149 transcription (Figure 1D, upper right quadrant), 2. genes that change only in stability (Figure 1D,
150 lower right quadrant), 3. genes that change only in transcription (Figure 1D, upper left quadrant)
151 and 4. genes that change in neither (Figure 1D, lower left quadrant). Thus, using this methodology,
152 we identified 213 genes with a statistically significant change in stability (Figure 1D lower right



153 quadrant). We were also able to identify a set of 2,834 genes with evidence for no change in stability
 154 under our experimental conditions (Figure 1D lower left quadrant) and 19,744 genes we have have
 155 insufficient information to reliably classify. Additionally, we show only one gene, *ETV1*, with
 156 a statistically significant change in transcription, 11,527 genes with statistically significant lack
 157 of change in transcription and 11,263 genes we have insufficient information to reliably classify.
 158 Taken together and consistent with the Pumilio proteins' role in post-transcriptional regulation,
 159 these results suggest that PUMs regulate gene expression at the level of RNA stability and not
 160 transcriptional initiation. Furthermore, this analysis allows us to divide the genes into those in
 161 which Pumilio knockdown has an effect on RNA stability and those in which there is evidence
 162 for a lack of effect on RNA stability, a stronger statement than simply failing to reject the null
 163 hypothesis that no change was occurring. The words EFFECT and NOEFFECT will be used to
 164 refer to these respective gene classes throughout the rest of the paper.

Figure 1 (previous page): Bru-seq and BruChase-seq allow for determination of PUM-mediated effects on RNA stability. A) Experimental design for measuring PUM-mediated effects on RNA stability. HEK293 cells incubated for 30 minutes in the presence of 2mM BrU prior to time 0. Cells were then washed and cultured in media containing 20 mM unlabeled uridine for six hours. At 0 and 6 hour timepoints, a portion of cells were harvested and BrU labeled RNA was isolated for sequencing. Changes in relative RNA abundance between the 0 and 6 hour time points were compared between cells grown in the presence of silencing RNA targeting *PUM1* and *PUM2* (siPUM) and a non-targeting control siRNA (NTC). Cells were treated with siRNAs for 48 hours prior to BrU labeling to allow for PUM depletion. B) Read coverage traces for *CCNG2* as measured in reads per million (RPM). Traces are shown for siPUM (orange) and NTC (blue) conditions at both 0H (top) and 6H (inverted bottom) time points. Four replicates for each combination of siRNA and time point are overlaid. Known isoforms for *CCNG2* are represented above. C) (Top) Volcano hexbin plot displaying global changes in RNA stability under PUM knockdown conditions. Stability in PUM knockdown is represented by a normalized interaction term between time and condition, where positive values indicate stabilization upon PUM knockdown and negative values indicate destabilization upon PUM knockdown (see Methods for details). No change in stability is represented with a dotted line at 0. Statistical significance at an FDR corrected p-value < 0.05 is represented with a horizontal dashed line. A selection of genes known to be regulated by PUM [34, 35] and genes newly identified in this study are labeled. For selected genes only, red triangles indicate genes that have a PRE in any annotated 3' UTR as determined by a match to the PUM1 motif we identified using SEQRS (Figure 2A). Gray squares indicate genes that did not have a PRE in their 3' UTR. Unlabeled genes are binned into a two-dimensional histogram to avoid overplotting. (Bottom) Marginal distribution of Stability in PUM knockdown for genes with a PRE in their 3' UTR (red) and genes without a PRE in their 3' UTR (gray). Median values for each distribution are plotted as a dashed line in the appropriate color. The star indicates a statistically significant difference in the median stability as measured by a two-sided permutation of shuffled labels ($n = 1000$, $p < 0.001$). D) Analysis of changes in transcription vs. changes in stability. Four separate statistical tests were calculated for each gene: 1. a test for statistically significant changes in RNA stability (Δ Stability $\neq 0$), 2. a test for statistically significant changes in transcription (Δ Txn $\neq 0$), 3. a test for no change in RNA stability (Δ Stability = 0), and 4. a test for no change in transcription (Δ Txn = 0). Genes are plotted as an (x,y)-coordinate where each coordinate represents the $\pm \log_{10}$ (FDR corrected p-value) of the test with greater evidence ($\Delta \neq 0$, $+\log_{10}$; or $\Delta = 0$, $-\log_{10}$) for each axis (see Methods for details). Representative genes displaying a range of stability effects are labeled. Red squares represent genes that were destabilized in PUM knockdown, whereas red triangles represent genes that were stabilized in PUM knockdown. All other genes were binned into a two dimensional histogram. Gray rectangles represented a statistical significance cutoff of q-value > 0.05 . (Left and Below) Marginal histograms for each axis are plotted with matching gray rectangles to represent the same statistical significance cutoff of q-value > 0.05 .

165 2.2. SEQRS shows conserved preference for the canonical UGUANAUA PRE by Pumilio proteins

166 The sequence preferences for both the full length PUM1 and PUM2 have been previously probed
167 *in vivo* [36–38, 50] and the sequence preferences for the RNA-binding domains of both PUM1 and
168 PUM2 were probed *in vitro* [10, 51, 52]. Each of these approaches and methodologies agree on a
169 general preference for the UGUANAUA consensus motif for both PUM1 and PUM2, with subtle
170 differences in the information content for the Position Weight Matrices (PWM)s obtained from
171 each technique, particularly at the 3' end of the PWM. However, prior *in vitro* determination
172 of human PUM sequence preferences have involved only one round of selection [51] or a selected
173 subset of possible sequences [52]. Thus, to compare the binding specificity of the PUM-HD of
174 the human PUM1 and human PUM2 proteins we applied *in vitro* selection and high-throughput
175 sequencing of RNA and sequence specificity landscapes (SEQRS) to purified PUM-HDs of each
176 protein [53]. Similar to systematic evolution of ligands by exponential enrichment (SELEX) [54],
177 SEQRS allows for the determination of an RNA-binding protein's sequence specificity by selecting
178 for RNAs that interact with the RBP out of a pool of random 20mers generated by T7 transcription
179 of a synthesized DNA library. The RNA pulled-down from a previous round is reverse-transcribed
180 into DNA to be used as the input for the next round of transcription and selection, allowing for
181 exponential enrichment of preferred sequences for any RBP of interest. We applied five rounds of
182 SEQRS to the PUM1 and PUM2 PUM-HDs separately and quantified the abundance for each of
183 the 65536 possible 8mers in the sequencing libraries for each round (including 8mers that would

184 overlap with the adjacent static adapter sequences see Methods for details).

185 To obtain representative PWMs for each round of selection (Figure 2A,B (top)), we used the top
186 enriched 8mer, UGUAAAUA, as a seed sequence to create a multinomial model from the abundance
187 of every possible single mismatched 8mer to the seed sequence (see Methods for details). This data
188 analysis approach has yielded similar results to that of expectation-maximization algorithms such as
189 MEME [55] and has been used successfully with SELEX experiments using DNA-binding proteins
190 [56, 57]. We also applied this same analysis pipeline to previously published SEQRS analysis of the
191 *D. Melanogaster* Pumilio PUM-HD [53] and find that it readily captures the *D. mel* Pum sequence
192 preference for the canonical UGUANAUA PRE (Figure 2D (top)). However, the PWMs defined
193 here (Figure 2A,B,D (top panels)) are representative of only the most highly enriched sequences in
194 each dataset and round.

195 In order to determine how representative the UGUANAUA consensus motif is for the entire
196 dataset of each protein, we grouped each 8mer based on its similarity to the UGUAAAUA seed
197 sequence as measured by the number of mismatches to that seed (Hamming distance). We then
198 considered the relative enrichment of a given 8mer within each round compared to its relative en-
199 richment within the input pool. Thus, scores above 0 indicate higher relative abundance than the
200 input pool for a given 8mer and scores below 0 indicate lower relative abundance. Here, we see that
201 8mers within 1-2 mismatches of the UGUAAAUA seed sequence are highly enriched compared to
202 8mers with more than 2 mismatches across each round for each protein (Figure 2A,B,D (bottom)).
203 However, the high level of variation in enrichment scores with higher numbers of mismatches and
204 the inclusion of some 8mers with high enrichment scores in these groups, suggests that only con-
205 sidering sequences that are within 1 or 2 mismatches of the canonical PRE (here represented by
206 UGUAAAUA) may not fully describe PUM binding specificity. Additionally, the PWM we ob-
207 tained from our SEQRS experiment for PUM2 PUM-HD (Figure 2B-C) suggests that the PUM2
208 has much weaker enrichment for the canonical PUM PRE compared to PUM1, which is inconsistent
209 with PUM2 sequence preferences obtained from *in vivo* transcriptome-wide experiments [36, 37].
210 This may indicate differences between *in vitro* and *in vivo* conditions that specifically impact PUM2
211 or may indicate that PUM2 PUM-HD does not bind as efficiently to RNA as the full-length PUM2
212 protein. However, comparing PWMs between these two proteins only considers the most highly
213 enriched sequences in each dataset. As seen in Figure 2C, the consensus motif emerging from the
214 PUM2 SEQRS data strongly resembles those for other PUMs, albeit with less apparent stringency.

215 To compare the overall sequence preferences between PUM1 and PUM2 we plotted the enrich-
216 ment scores for all possible 8mers in each dataset against each other (Figure 2E). We find that the
217 8mer enrichment scores between these two proteins are highly correlated (Spearman's $\rho = 0.63$)
218 which indicates that PUM1 and PUM2 PUM-HDs have overall similar sequence preferences when
219 considering all possible sequences rather than highly enriched sequences. We also see that the PUM1
220 PUM-HD has an overall stronger enrichment for highly enriched sequences compared to PUM2,
221 which may explain the differences in obtained PWMs for each protein. When considering only the
222 8mers within one mismatch to the UGUAAAUA seed sequence used for creating the PWMs, we
223 find that enrichment scores between PUM1 and PUM2 are nearly perfectly correlated (Spearman's
224 $\rho = 0.91$). Furthermore, mismatches in the 3' end of the motif appear to be less detrimental to
225 enrichment by PUM1 and PUM2 compared to mismatches in the 5' end of the motif, which is
226 also represented by the lower information content at the 3' end of the PWMs. Due to the overall
227 similarity in sequence preferences between these two proteins and the higher overall information
228 content in the PUM1 PWM, the SEQRS round 5 PWM for PUM1 will be used to determine PREs
229 throughout the text, unless otherwise indicated.

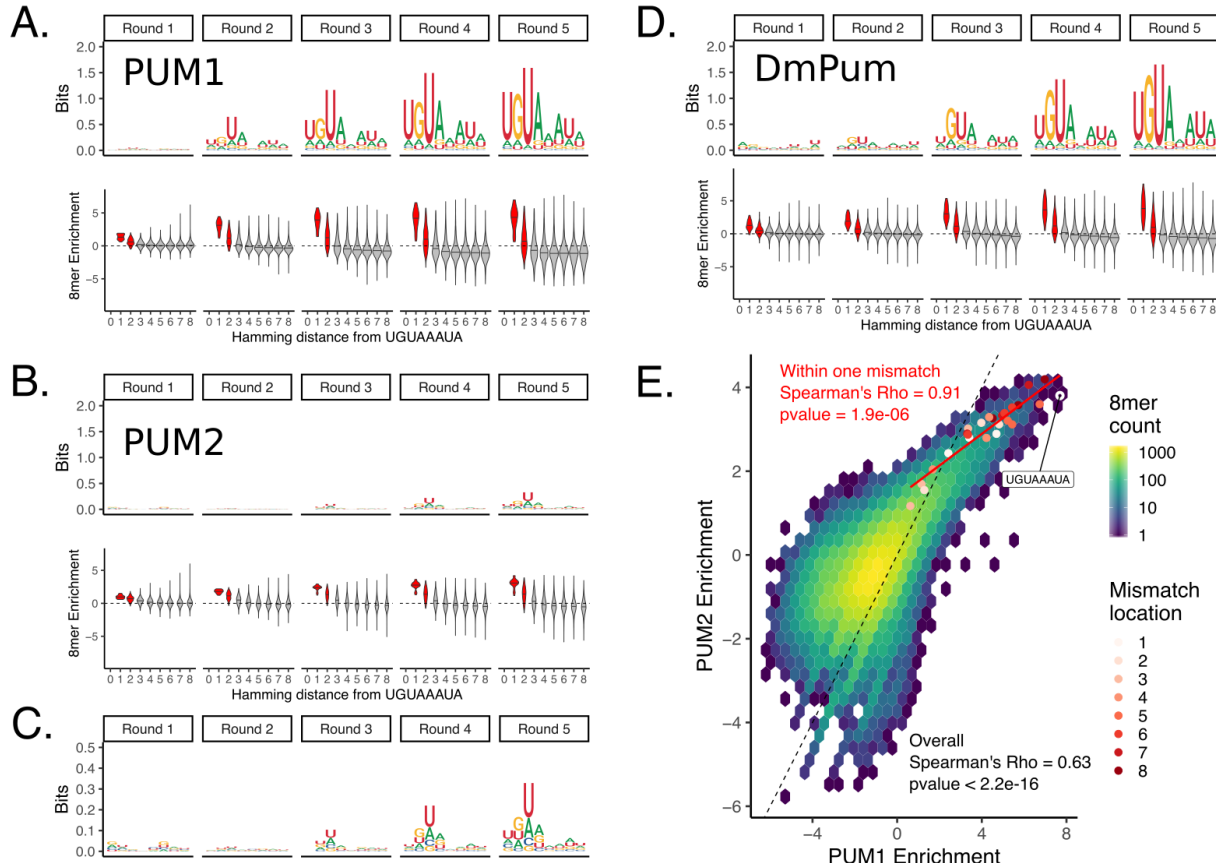


Figure 2: SEQRS analysis of Human PUM1 and PUM2 PUM-HDs reveals preference for the canonical PUM Recognition Element. A) (Top) Position weight matrices representing 8mer sequence preferences for purified Human PUM1 PUM-HD, as determined for each SEQRS round. (Bottom) 8mer enrichment, as measured by $\log_2(\text{Enrichment SEQRs round} / \text{Enrichment no protein})$ (see Methods for details) for each 8mer as binned by Hamming distance from the canonical UGUAAAUA PUM recognition element. Enrichment scores for 8mers within 2 mismatches are filled in red. B) Same as in A, but for Human PUM2 PUM-HD. C) Closer view of Human PUM2 PUM-HD PWMs. D) Same as in A, but for Drosophila Pum PUM-HD. E) Correlation of 8mer enrichment between Human PUM1 and Human PUM2 PUM-HDs. Enrichment for all possible 8mers are displayed in a two dimensional histogram. The dashed black line represents one to one correspondence. All 8mers within one mismatch to the UGUAAAUA sequence are plotted as red points with the color specifying the position within the motif where the mismatch occurs. The red line is a linear fit using only the UGUAAAUA 8mer and all 8mers within one mismatch.

230 2.3. Contextual features around PREs are associated with PUM-mediated RNA stability effects

231 Determining what distinguishes a functional binding site from a non-functional binding site is a
232 major question for any RBP. Taken as a whole, RBPs tend to bind similar low sequence complexity
233 motifs *in vitro* [51]. Additionally, probing of RBP binding *in vivo* at a transcriptome-wide scale,
234 has indicated that the majority of predicted binding sites are not bound for some RBPs [58].
235 Global *in vivo* experiments with the Pumilio-family of proteins have established that mammalian
236 Pumilio proteins recognize the UGUANAUA PRE in the 3' UTR of target genes [22, 32, 36, 37].
237 However, predicting the PUM-mediated effect on gene expression from sequence information and/or
238 PUM-binding measurements remains an elusive goal [34].

239 To determine sequence motifs *de novo* that have explanatory power for our RNA stability
240 dataset, we used FIRE [59] to find motifs in the 3' UTR of transcripts that share high mutual
241 information with our RNA stability dataset by taking the normalized interaction term (see Methods
242 for details) and discretizing it into ten bins, with an equal number of genes in each bin. Figure 3A
243 shows that FIRE rediscovers the canonical UGUANAUA PRE using only the RNA stability data
244 as input. Furthermore, the UGUANAUA PRE is enriched in transcripts that are highly stabilized
245 under PUM knockdown conditions, suggesting that these transcripts are regulated by PUM through
246 recognition of a UGUANAUA PRE in their 3' UTR.

247 To determine whether there was evidence for PUM binding at PREs associated with a change
248 in RNA stability, we used publicly available *in vivo* binding data for human PUM2 obtained using
249 photoactivatable ribonucleoside-enhanced crosslinking and immunoprecipitation (PAR-CLIP) [37].
250 The PAR-CLIP technique involves incorporation of 4sU into the total cellular RNA pool allowing
251 for efficient crosslinking of proteins that bind near an incorporated 4sU. Upon creation of sequencing
252 libraries from PAR-CLIP samples, a T → C mutation is induced at the crosslinking site which can
253 be used as additional evidence for a protein binding. We used PAR-CLIP data from Hafner et al.
254 [37] to determine the amount of binding signal at PREs associated with transcripts that have a
255 statistically significant change in RNA stability under PUM knockdown (EFFECT class, Figure
256 1D) and compared it to transcripts with a statistically significant lack of change in RNA stability
257 (NOEFFECT class, Figure 1D). In Figure 3B, we report the average PAR-CLIP read coverage
258 in a 40 bp window around PREs in the 3' UTR of transcripts associated with the EFFECT and
259 NOEFFECT classes. We use a 5% truncated mean to remove the impact of extreme outliers on
260 the average coverage reported. To estimate a 95% confidence interval on the average coverage
261 (shaded region), we performed bootstrapping ($n = 1,000$) by sampling vectors of read coverage for
262 individual PREs with replacement. Here, we clearly see that PREs in transcripts with a change
263 in RNA stability have higher binding signal than those with no change in RNA stability. This is
264 consistent with higher overall PUM binding at PREs associated with changes in RNA stability but,
265 as the PAR-CLIP signal is not normalized to RNA abundance, the possibility that these transcripts
266 were simply more abundant under the PAR-CLIP conditions cannot be definitively ruled out.

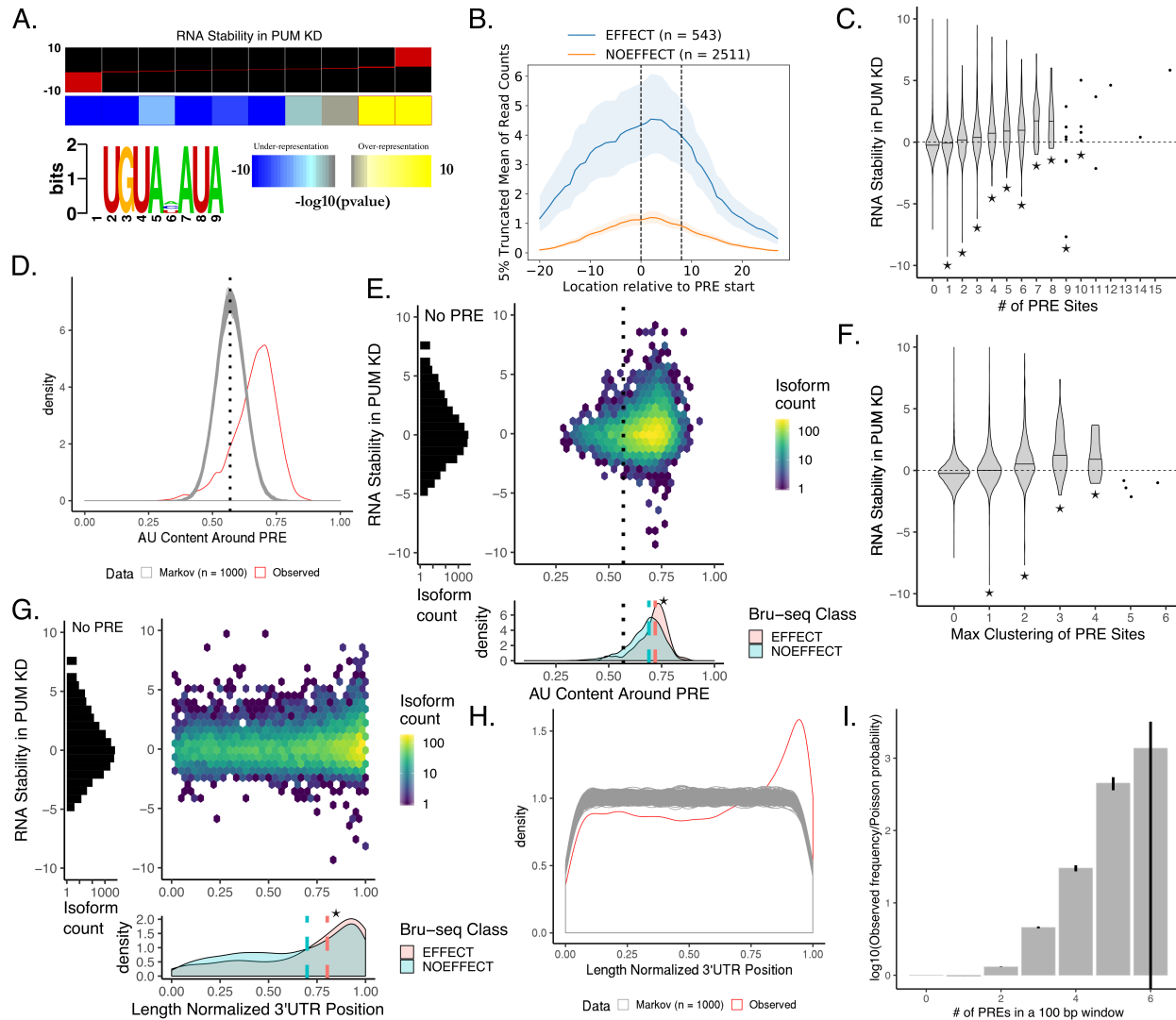
267 We have shown that a PRE in the 3' UTR is associated with a change in RNA stability under
268 PUM knockdown and that PREs in transcripts with a change in RNA stability have evidence for
269 being bound by PUM *in vivo*. However, knowledge of the presence or absence of a PRE in the
270 3' UTR alone is not sufficient to predict the magnitude of PUM-mediated repression, and a wide
271 variation in the effect of knocking down human PUM1 and PUM2 on steady-state RNA levels has
272 been observed in previous transcriptome-wide analysis [34]. Here, we demonstrate that a similar
273 level of variation can be seen in measurements of RNA stability. Figure 3C displays the overall
274 distribution of RNA stability measurements for transcripts with increasing numbers of PREs in
275 annotated 3' UTRs. We find that an increase in the number of PREs is, on average, associated
276 with an increase in RNA stability under PUM knockdown conditions compared to transcripts that
277 do not have a PRE in their 3' UTR. However, wide variations in RNA stability can be seen for

278 each category, consistent with previous measurements of changes in steady state RNA levels under
279 PUM knockdown [34]. Thus, a simple count of PREs does not fully explain PUM-mediated action
280 at a particular transcript.

281 To explore the local sequence context around PREs, we trained a 3rd order Markov model on
282 the full set of unique annotated human (hg19) 3' UTRs that were greater than 3 basepairs long
283 (29,380 3' UTRs). Using this Markov model, we simulated 1,000 different sets of 29,380 3' UTRs
284 that were the same length and shared similar sequence composition to the set of true 3' UTRs.
285 We then searched for matching PREs in the simulated sets of 3' UTRs and calculated the AU
286 content in a 100 bp window around these PREs. On average, we discovered 12200 matching PREs
287 (standard deviation of 112) in simulated sets of 3' UTRs compared to the 14086 matching PREs
288 in the annotated set of 3' UTRs. We find that the true set of PREs have, on average, higher local
289 AU content than PREs in simulated sets of 3' UTRs (Figure 3D). Additionally, in the simulated 3'
290 UTRs the local AU content for PREs is centered around the average AU content for all 3' UTRs,
291 as would be expected if there was no selective pressure for PREs to occur in AU rich areas of 3'
292 UTRs. This analysis is consistent with Jiang et al. [60] who also observed a preference for PREs
293 to occur in AU rich areas as compared to shuffled PREs with preserved overall sequence content.
294 Here we further show that the local AU content surrounding a PRE is associated with a functional
295 effect on PUM-mediated regulation.

296 To determine the relationship between local AU content and changes in RNA stability upon
297 PUM knockdown, we plotted the AU content of a 100 bp window surrounding a PRE within a gene's
298 3' UTR against the corresponding RNA stability measurement for that gene (Figure 3E top). For
299 3' UTRs with more than one PRE, the PRE with the highest local AU content was considered. We
300 find that large changes in RNA stability are associated with higher local AU content. Additionally,
301 PREs in transcripts that had a statistically significant stability effect in PUM knockdown had
302 higher local AU content compared to PREs in transcripts with no change in stability ($p < 0.001$,
303 Figure 3E bottom). These data indicate that local sequence context beyond the PRE plays a role
304 in PUM function.

305 Previously proposed mechanisms of PUM-mediated control of RNA stability involve interaction
306 with the CCR4-NOT complex and/or PABPs, both of which act at the 3' end of mRNA transcripts
307 to promote deadenylation or participate in translation initiation [32, 33]. Thus, the location of PUM
308 binding sites within the 3' UTR of target transcripts may play a role in determining PUM-mediated
309 effects on stability by physically locating PUM near known co-regulators. Using the Markov models
310 described above, we also determined the location of PREs within 3' UTRs. As shown in Figure
311 3H, we observe that the observed distribution of true PRE locations in length-normalized 3' UTRs
312 appear enriched towards the 3' end of 3' UTRs (red) as compared to PREs found within 1000
313 simulated sets of 3' UTRs (gray). Again, this suggests a selective pressure for PRE sites to exist at
314 the 3' end of 3' UTRs as compared to the uniform distribution of PREs found in simulated 3' UTRs
315 with similar sequence properties. Like the AU content analysis, this analysis is also consistent with
316 observations made by Jiang et al. [60] who saw an enrichment towards the 3' end for PRE locations
317 in the full set of human 3' UTRs compared to a shuffled PRE motif with preserved overall sequence
318 content. While these approaches are complementary, our approach allows for the exact identity of
319 the PRE to remain intact thereby maintaining a PRE-centric assessment rather than one based
320 solely on the general sequence content within the motif. Additionally, we observe that transcripts
321 with a PRE towards the 3' end of the 3' UTR tend to have a larger RNA stability effect (Figure
322 3G center) and PREs in transcripts that had a statistically significant change in stability in PUM
323 knockdown were, on average, closer to the 3' end of the 3' UTR than those with no change in RNA
324 stability ($p < 0.001$, Figure 3G bottom), suggesting a functional role for PRE location in the 3'
325 UTR of target transcripts.



326 High throughput analysis of many human RBPs has indicated that some RBPs prefer to bind
 327 bipartite motifs, suggesting that clustering of RBP binding sites may contribute to binding speci-
 328 ficity and subsequent function [51]. To determine the relationship between PRE clustering and
 329 RNA stability in PUM knockdown, we discretized transcripts according to the maximum number
 330 of complete PREs that were within a sliding 100 bp window in the 3' UTR of a transcript and
 331 plotted the distribution of RNA stability measurements for each cluster (Figure 3F). Similar to
 332 the association with the number of PREs (Figure 3C), we find that having more PREs clustered
 333 together is associated, on average, with a higher stabilization effect under PUM knockdown con-
 334 ditions. We also find that PREs tend to cluster together more than one would expect by chance by
 335 determining the divergence from a simple Poisson model (Figure 3I, $p < 0.001$ for clusters 2-5; see
 336 Methods for details). Taken together, this analysis suggests that clustering of PREs may facilitate
 337 PUM action on target transcripts.

Figure 3 (previous page): Features associated with a PUM Recognition Element (PRE) explain some variability in PUM-mediated effect on decay. A) Results of motif inference using FIRE [59] on the stability in PUM knockdown data discretized into 10 equally populated bins. Red bars within each bin represent the spread of RNA stability values within each bin. Stability in PUM knockdown is represented by a normalized interaction term between time and condition throughout this figure, where positive values indicate stabilization upon PUM knockdown and negative values indicate destabilization upon PUM knockdown (see Methods for details). B) 5% truncated average of Pum2 PAR-CLIP read coverage [37] over each PRE site in the 3' UTRs of genes with a statistically significant change in RNA stability (blue) compared to genes in which there was a statistically significant lack of change in stability (orange; see Methods for details on NOEFFECT test). Shaded regions represent bootstrapping ($n = 1,000$) within each group. Dashed lines indicate the PRE site. C) Violin plots representing the distributions of RNA stability for genes with 0 to 15 PRE sites within their 3' UTR. Stars represent statistical significance as measured by a Wilcoxon rank sum test using equality of pseudomedian with the 0 PRE case as the null hypothesis. D) Distribution of AU content in a 100 bp window around all unique PRE sites in the 3' UTRs of the human transcriptome. The observed distribution (red) is compared to the distribution of AU content around PRE sites in 1,000 simulated sets of 3' UTRs the same size as the true set of 3' UTRs as simulated from a third order Markov model trained on the true 3' UTR sequences. The dotted line represents the average overall AU content of the entire set of 3' UTRs in the human transcriptome. E) Relationship of AU content in a 100 bp window around a PRE to RNA stability. (left) Marginal histogram of RNA stability for genes with 0 PREs in their 3' UTRs. (right) 2D histogram of RNA stability and AU content around each PRE site for all genes with at least one PRE in the 3' UTR. Dotted line represents the average AU content over the entire set of 3' UTRs in the human transcriptome. (bottom) Marginal kernel density plot of AU content around a PRE site split amongst genes with a statistically significant change in RNA stability (red) and genes with a statistically significant lack of change in stability (blue). Dotted black line represents the average AU content of 3'UTRs. Dashed lines represent the median AU content around a PRE for the EFFECT (red) and NOEFFECT (blue) genes. The star represents a statistically significant difference in medians using a one-sided permutation test ($n=1,000$) of shuffled class labels. F) Violin plots representing the distributions of RNA stability for genes with 0 to 6 full PRE sites clustered within a 100 bp window. Stars represent statistical significance as measured by a Wilcoxon rank sum test using the 0 PRE case as the null distribution. G) Relationship of normalized location of PRE site in 3' UTR to RNA stability. Plots as in (D). H) Distribution of length normalized locations of PRE sites in the 3' UTRs of the human transcriptome. The observed distribution (red) is compared to that of PRE sites found in 1,000 simulated sets of 3' UTRs calculated as in (G). I) Comparison of the observed frequencies of PRE site clustering over all possible 100 bp windows in the full set of human 3' UTRs with at least 1 PRE in them to the probabilities expected from a Poisson null distribution. Error bars represent 95% confidence intervals based on 1,000 bootstraps of the observed distribution.

338 2.4. *Pumilio proteins modulate the stability of genes involved in neural development, cell signaling,*

339 and gene regulation

340 Mammalian Pumilio proteins have been shown to regulate a diverse set of genes, including those

341 involved in signaling pathways, transcriptional regulation, and neurological functions [18, 22, 23,

342 34, 35]. Consistent with prior observations, we see changes in RNA stability for genes involved

343 in these functions. For example, multiple epidermal growth factor-like-domains 9 (*MEGF9*) is a

344 transmembrane protein that is highly expressed in the central and peripheral nervous system and

345 its expression appears to be regulated during nervous system development in mice [61]. We see

346 strong stabilization of the *MEGF9* transcript under PUM knockdown conditions (Figure 4A top).

347 Furthermore, of the five PREs we identify in two unique 3' UTRs for *MEGF9*, we see the most

348 PUM2 binding signal for the 3'-most PRE (Figure 4A bottom right). Additionally, we see that the

349 3'-most PRE has high local AU content compared to the overall distribution of PRE sites (Figure 4A

350 bottom left). Taken together, these data implicate the PUM proteins as direct post-transcriptional

351 regulators of *MEGF9*.

352 Another transcript that is strongly stabilized under PUM knockdown conditions is glycogen

353 synthase kinase-3 B (*GSK3B*) (Figure 4B top). *GSK3B* is a serine-threonine kinase that is involved

354 in the regulation of diverse cellular processes and its misregulation is associated with neurological

355 disease [62, 63]. We identify four PREs in *GSK3B* 3' UTRs (Figure 4B below) with largely similar

356 adjacent AU content (Figure 4B bottom left). We also find that the 3' most distal PRE has evidence
357 for PUM2 binding consistent with the global trends we describe in Figure 3. Like *MEGF9*, this
358 evidence suggests that PUM proteins are involved in destabilizing *GSK3B* transcripts.

359 We also see examples of RNAs that are destabilized when PUM is knocked down, suggesting
360 that PUM may actually act to stabilize these transcripts under conditions containing WT levels of
361 PUM expression. Transcription dimerization partner 2 (*TFDP2*) encodes a protein that cooperates
362 with E2F transcription factors to regulate genes important for cell cycle progression; dysregulation
363 of this system can lead to cancer [64]. PUM proteins have been previously shown to regulate another
364 member of the E2F family by functionally cooperating to enhance the effect of miRNA-mediated
365 regulation of *E2F3* expression [65]. Furthermore, regulation of *TFDP2* by the liver-specific miRNA
366 *miR-122* has been shown to be important for preventing up-regulation of *c-Myc* in hepatic cells
367 [66]. We observe that *TFDP2* is highly destabilized under PUM knockdown conditions (Figure 4C
368 top). Additionally, we find that the *TFDP2* 3' UTR has a single PRE site toward the 3' end of
369 the 3' UTR and has high adjacent AU content (Figure 4C bottom and lower left). However, there
370 is limited evidence for PUM2 binding in PAR-CLIP data (Figure 4C lower right). One possible
371 mechanism for PUM mediated activation of *TFDP2* is by acting to block regulation by miRNAs;
372 however, the nearest conserved miRNA site of a conserved miRNA family to the PRE is over 100
373 bases away [67] and further evidence would be needed to establish this link.

374 Another example of a highly destabilized transcript under PUM knockdown conditions is the
375 embryonic lethal abnormal vision 1 (*ELAVL1*) or HuR RNA-binding protein (Figure 4D top).
376 The *ELAVL1* RBP stabilizes RNA transcripts by binding to AU-rich elements in the 3' UTR of
377 transcripts [68] and its dysregulation is associated with several different types of cancer [69]. We
378 found one PRE in the 3' UTR of *ELAVL1* (Figure 4D bottom). This motif is found towards the
379 3' end of the 3' UTR but has average local AU enrichment compared to other PREs found across
380 all annotated 3' UTRs (Figure 4D lower left). Additionally, there is limited evidence for binding
381 by PUM2 at either of the PREs in the *ELAVL1* 3' UTR (Figure 4D lower right). Taken together,
382 this suggests that *ELAVL1* may be indirectly regulated by PUM.

383 To discover categories of genes that are globally associated with RNA stability changes in PUM
384 knockdown, we applied iPAGE—a computational tool that uses mutual information to find in-
385 formative Gene Ontology (GO) terms associated with discretized gene expression data [70]—to
386 our stability dataset as represented by the normalized interaction term discretized into 5 equally
387 populated bins. It is worth noting that this analysis will discover pathways regulated both indi-
388 rectly and directly by PUM out of the full set of annotated GO terms. Figure 5A displays the
389 iPAGE results with several GO terms that are either significantly overrepresented (red-filled box)
390 or underrepresented (blue-filled box) across the full range of stability data. We see several enriched
391 GO term categories that are consistent with previous reports of changes in steady-state RNA lev-
392 els under PUM knockdown in HEK293 cells [34] including categories related to guanyl-nucleotide
393 exchange factor activity (GO:0005085), WNT signaling (GO:0030177), nucleosome (GO:0000786)
394 and platelet-derived growth factor receptor signaling (GO:00048008).

395 For a finer grain view, we plotted the RNA stability results for each gene involved in selected
396 GO terms as indicated by either blue (destabilized in PUM KD) or red (stabilized in PUM KD)
397 text for that GO term in Figure 5A. In Figure 5B, we show two selected GO terms whose members
398 tend to be de-stabilized upon PUM knockdown: nucleosome (GO:0000786, left) and myelin sheath
399 (GO:0043209, right). For genes related to the nucleosome, we see a general destabilization under
400 PUM knockdown conditions. However, when comparing genes within this GO term that have a
401 PRE in their 3' UTR to those that do not, we see that genes with a PRE in their 3' UTR have
402 a median stability upon PUM KD that is significantly higher than those without a PRE in their
403 3' UTR ($p < 0.001$), suggesting that the destabilization of most nucleosome genes under PUM

404 knockdown conditions may be mediated indirectly. Some of these effects could be explained by
405 perturbation of the stem-loop binding protein (SLBP), as SLBP is a protein involved in the proper
406 maturation of replication-dependent histone mRNAs [71], and we observe that *SLBP* is significantly
407 stabilized under PUM knockdown conditions (Figure 1C).

408 PUM knockdown also causes a general de-stabilization of genes categorized into the myelin
409 sheath GO term. A role for PUM in controlling the stability, either indirectly or directly, of genes
410 involved in the myelin sheath is consistent with the previously identified role of mammalian PUMs
411 in neurogenesis and neurodegenerative diseases [19, 22, 23, 31]. However, we see no evidence for
412 a difference in stability between genes that have a PRE in their 3' UTR compared to genes that
413 do not have a PRE in their 3' UTR. Furthermore, the genes that have a statistically significant
414 de-stabilization under PUM knockdown have no PRE in their 3' UTR, whereas the genes with a
415 significant stabilization do, suggesting a complex role of PUM in modulating the stability of genes
416 in this GO term, possibly arising mainly through indirect effects.

417 In Figure 5C, we report specific GO terms that were enriched in genes that were stabilized
418 under PUM knockdown and thus likely contain many classic, PUM-repressed targets. Consistent
419 with this idea, we find that each of these GO terms represent classes of genes that have previously
420 been associated with PUM-mediated regulation. For instance, the guanyl-nucleotide exchange
421 factor activity GO term (GO:0005085; Figure 5C, far-left) includes guanine nucleotide exchange
422 factors (GEFs) which activate Rho-family GTPases to regulate a diverse suite of cellular functions,
423 including cell-cycle progression, the actin cytoskeleton, and transcription [72]. Additionally, genes
424 involved in peptidyl-serine phosphorylation (GO:0018105; Figure 5C, mid-left), represent a broad
425 class of kinases, including those involved in neurological disease and inflammation [63, 73]. Finally
426 genes involved in transcriptional repressor activity (GO:0001078, Figure 5C, mid-right), include
427 proteins involved in regulating hematopoiesis and controlling neurological development [74–76].
428 Supporting the idea that PUMs are directly repressing subsets of genes within these GO terms
429 we find that, for each GO term above, genes with a PRE in their 3' UTR are significantly more
430 stabilized under PUM knockdown than those with no PRE.

431 Of particular interest is the mild enrichment of genes that were stabilized under PUM knock-
432 down for the CCR4-NOT complex GO term (GO:0030014; Figure 5C, far-right). Almost every
433 gene in this GO term was stabilized under PUM knockdown to some extent. Although the overall
434 effect of a PRE for genes in this category did not meet our threshold for statistical significance,
435 several of the genes have a PRE in their 3' UTR including both genes with a statistically significant
436 change in stability. Human Pumilio proteins have been shown to interact with the CCR4-NOT
437 complex and recruit the complex to target mRNAs for de-adenylation [32]. These data suggest
438 that PUM could also be acting to directly inhibit CCR4-NOT expression and thus globally lower
439 deadenylation rates, perhaps providing a feedback loop that further regulates PUM activity.

440 Overall, we observe that genes associated with GO terms that are stabilized under PUM knock-
441 down have a significant association with PREs suggesting that these GO terms contain mainly genes
442 that are direct targets of PUM. In contrast, we find that genes associated with GO terms that are
443 destabilized under PUM knockdown do not have a significant association with PREs, suggesting
444 that these GO terms contain mainly genes that are indirect targets.

445 *2.5. Conditional random forest models allow for prediction of PUM-mediated effects from sequence-
446 specific features*

447 A long standing goal in the study of RBPs is to predict that RBPs effect on a given transcript
448 from known features about possible targets. Previous models of PUM-mediated regulation have
449 reported modest performance based on the number of PREs in various locations across the trans-
450 script including the 5' UTR, CDS, and 3' UTR [34]. Here, we use a different approach, which

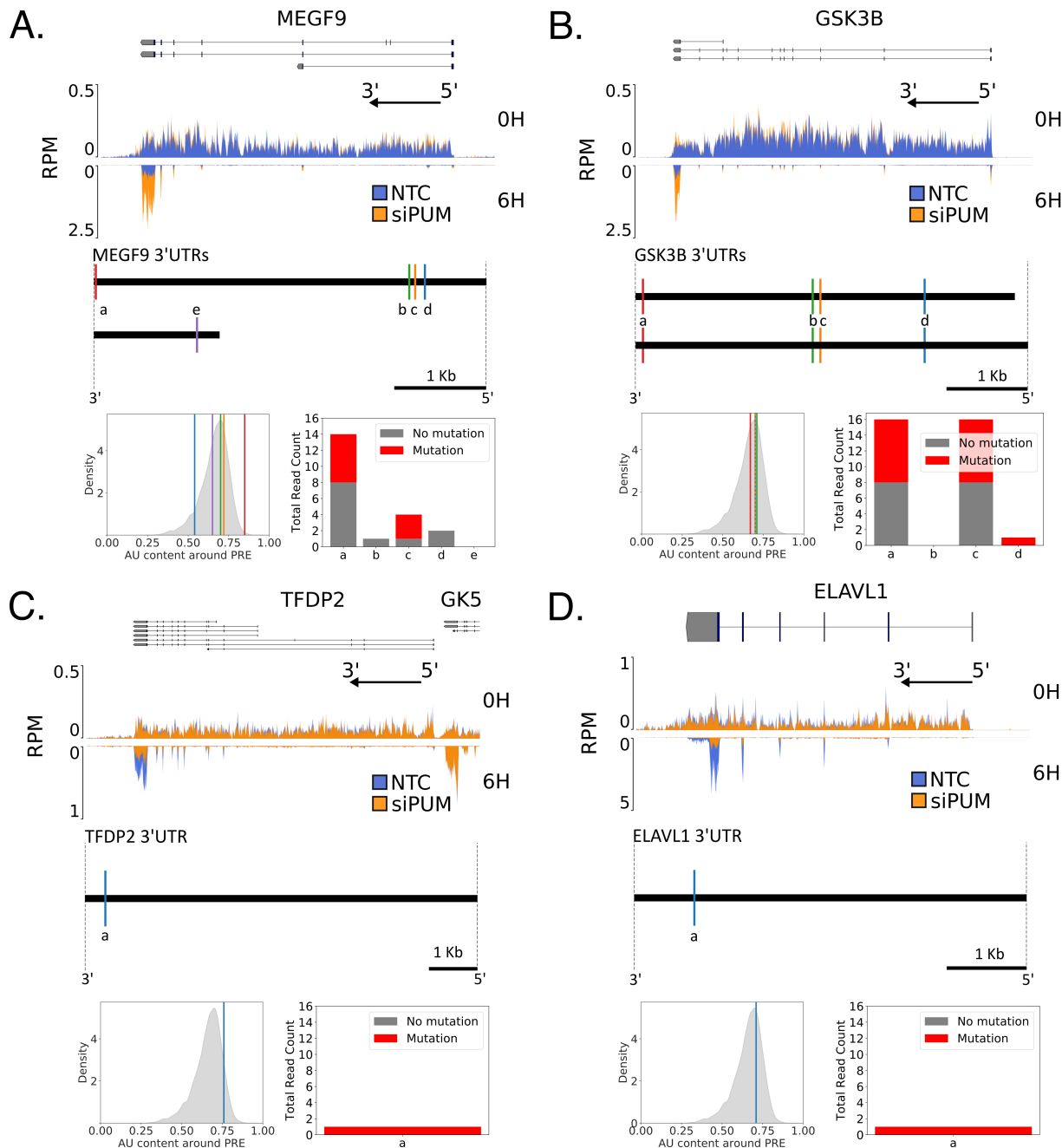


Figure 4: PUM-mediated effects on RNA stability under PUM knockdown include stabilization and destabilization. A) (top) Read coverage traces for *MEGF9* and surrounding region (chr9:123348195-123491765, hg19) as measured in reads per million (RPM). Traces are shown for siPUM (orange) and NTC (blue) conditions at both 0H (upper track) and 6H (inverted lower track) time points. Four replicates for each combination of siRNA and time point are overlaid. Known isoforms for *MEGF9* are represented above. The black arrow indicates the direction of the 5' and 3' ends of the transcribed RNA molecule from the gene shown. (Below) Diagram of unique *MEGF9* 3' UTRs. Sites matching the PUM1 SEQRS motif are represented as vertical lines and labeled alphabetically from 3' to 5' for each UTR. (Below left) AU content of a 100 bp window around each PRE labeled above in the overall distribution of surrounding AU content for all PUM1 SEQRS motif matches in the entire set of 3' UTRs. (Below right) PAR-CLIP read coverage [37] of 40 bp around each indicated PRE. Number of reads with a T→C mutation are shown in red, whereas the number reads with no T→C mutation are shown in gray. B) As in A), but for *GSK3B* and surrounding region (chr3:119509500-119848000). C) As in A), but for *TFDP2* and surrounding region (chr3:141630000-141900000). Annotations for the 3' end of the *GK5* gene are included due to their proximity to the *TFDP2* 5' end. D) As in A), but for *ELAVL1* and surrounding region (chr19:8015000-8080000).

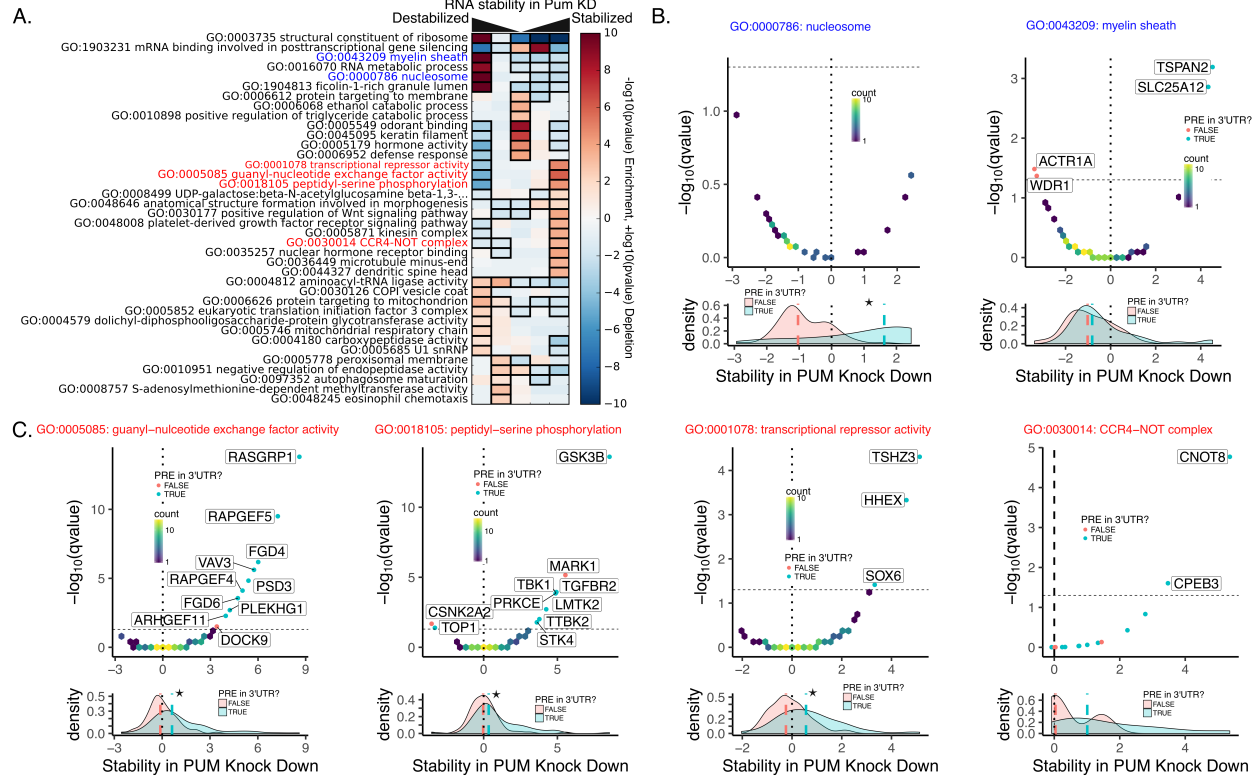


Figure 5: Gene ontology terms associated with PUM-mediated changes in RNA stability. A) Results of iPAGE analysis to find GO terms sharing mutual information with RNA stability discretized into 5 equally populated bins. Red bins indicate over representation of genes associated with the corresponding GO term. Blue bins indicate under representation of genes associated with the corresponding GO term. A black box indicates a statistically significant over or under representation with a p -value < 0.05 using a hypergeometric test [70]. Throughout this figure stability in PUM knockdown is represented by a normalized interaction term between time and condition, where positive values indicate stabilization upon PUM knockdown and negative values indicate destabilization upon PUM knockdown (see Methods for details). B) Selected GO terms whose members are over represented in the RNAs that are destabilized under PUM knockdown, as labeled in blue in panel A. For each GO term, a volcano plot is shown for all genes within the GO term. Volcano plots are shown as two dimensional histograms for genes below a statistical significance threshold (q -value < 0.05) and as individual points for genes above the statistical significance threshold. Individual points are blue if a PRE can be found within any annotated 3' UTR for that gene and red otherwise. The dashed line represents the statistical significance threshold and the dotted line represents no change in RNA stability under PUM knockdown. Below each volcano plot is a marginal density plot for the RNA stability split into two categories within the specified GO term: Genes with a PRE in any annotated 3' UTR (blue) and genes with no PRE in any annotated 3' UTR (red). Medians for each distribution are shown as dashed lines in the appropriate color. The black dotted line represents no change in RNA stability, as in the volcano plot above. A star represents a statistically significant ($p < 0.05$) difference in the medians as tested by a two-sided permutation test of shuffled group labels ($n = 1000$). C) As in (B), but for selected GO terms whose members are over represented in the RNAs that are stabilized under PUM knockdown, as labeled in red in panel A.

451 allows us to include a larger feature set of possible predictors for PUM-mediated regulation. Using
452 conditional random forest models [77], we divided genes into EFFECT and NOEFFECT classes,
453 as shown in Figure 1D. We used four different definitions for a PRE, (Figure 6A) including the
454 SEQRS motifs we defined for PUM1 and PUM2 in Figure 2A-B, the PUM2 motif determined from
455 Hafner et al. [37], and a regular expression (regex) representing UGUANAUW as defined from the
456 PUM consensus sequence which has been used extensively to define PREs in previous publications
457 [7, 34, 60]. We focused our analysis on PREs found in the 3' UTRs of target genes. For each
458 definition of a PRE, we calculated several features based on our analysis in Figure 3, including AU
459 content around a PRE, clustering of PREs, total count of PREs, a score for PRE match to the
460 specific PRE definition, relative location of the PRE in the 3' UTR, number of miRNA sites near a
461 PRE, and predicted secondary structure around a PRE. In addition to these features, we included
462 motif matches for additional human RBPs, *in vivo* PUM binding data, predictions of secondary
463 structure, and the fraction optimal codons for the CDS of target genes (see Methods for details).
464 As our data is highly unbalanced (199 EFFECT genes and 2535 NOEFFECT genes, after only
465 including genes that are present in all features) we trained 10 different machine learning models
466 where the NOEFFECT class was randomly downsampled to match the number of EFFECT class
467 genes in each model. Within each downsampled dataset, 5-fold cross validation was performed to
468 assess performance.

469 To determine which features best help predict EFFECT genes from NOEFFECT genes, we used
470 an AUC-based permutation variable importance measure [78], which indicates the average change
471 in the area under the curve (AUC) of a receiver operator characteristic (ROC) plot across all trees
472 with observations from both classes in the forest when the predictor of interest is permuted. By
473 permuting the feature of interest and measuring the change in AUC of the ROC curve, one can
474 measure the importance of that variable in predictive performance. Typically values of the AUC
475 of a ROC curve span from 0.5 to 1.0 where 1.0 indicates perfect classification performance and 0.5
476 indicates random guessing of class distinctions. Since the AUC-based variable importance measure
477 is calculated using the change in AUC when the predictor is permuted, the expected values are much
478 smaller and fall between 0.0 and 0.06 in simulated cases with 65 predictors and variable numbers of
479 observations from n=100 to n=1,000 [78]. Higher values indicate a larger drop in performance when
480 that variable is permuted; thus, the variables can be ranked based on their unique contribution
481 to the model, with higher values indicating a more important individual contribution. Figure 6B
482 displays the top 20 variables ranked according to their average AUC-based variable performance
483 across all 50 models (10 sets of downsampled models with 5-fold cross-validation each). Count
484 based metrics enumerating the total number of PREs within the 3' UTR appear to be the most
485 important variable for predicting a PUM-mediated effect in the Bru-seq and BruChase-seq data. In
486 addition, local AU content and PRE clustering appear to be substantial contributors to the models.
487 To a lesser extent, the number of miRNA sites around a PRE, the location of the PRE in the 3'
488 UTR, and the “Bound” status of the 3' UTR also appear to contribute meaningfully to our models.
489 It is possible that each of these variables contain largely the same information (i.e., whether or not
490 the 3' UTR has a PRE or not in it). Thus, in order to rule out the possibility that each feature was
491 simply differentiating between genes with a PRE in their 3' UTR from genes without a PRE, we
492 trained separate models for each motif definition where we only considered genes that have at least
493 one PRE present in their 3' UTR. Each of these models also displayed substantial contributions
494 for AU content, clustering, and total count in predicting PUM-mediated regulation, as measured
495 by Bru-seq and BruChase-seq (Figure S2A-D left panel) suggesting that each of these features are
496 contributing meaningful information to the model.

497 The high similarity in appearance between each of the definitions of a PRE we include here led
498 us to explore how much redundant information is contained between each of the top 20 highest

499 contributing features. To measure redundancy, we use an information theoretic definition based on
500 discretization of each feature (see Methods for details). In Figure 6C, we display the redundancy
501 between the top 20 features as a hierarchically clustered heatmap, where a value of 1.0 indicates
502 that the features contain exactly the same information and a value of 0.0 indicates that the fea-
503 tures share no information. Here, we can see that features that are defined around the same motif
504 definition or feature-type tend to share information (as expected). However, despite their similar-
505 ity in appearance, there are some differences in information content between the different motif
506 definitions and different feature types, indicating that there is knowledge to be gained outside of a
507 simple PRE count.

508 To assess the performance of our conditional random forest models we considered several typical
509 performance measures including summary metrics (Accuracy, F1 measure, Matthews correlation
510 coefficient [MCC], Area Under the Curve of a Precision-Recall Curve [AUC PRC], and AUC ROC),
511 and metrics more focused on performance for positive or negative cases (Negative Predictive Value
512 [NPV], Precision, Recall, Specificity). We considered each of these metrics for all 50 models (10
513 downsampled datasets with 5-fold cross-validation each) at a classification probability cutoff of 0.5.
514 The full range of values obtained are displayed in Figure 6D. It is evident that the models are
515 robust to both downsampling and cross validation and the performance hovers around 0.75 for
516 each metric (and 0.5 for MCC), indicating balanced performance in predicting both positive and
517 negative classes. These results are robust even in the case where we only use one PRE definition
518 and only consider genes that contain a PRE in their 3' UTR (Figure S2A-D).

519 In order to determine the predictive efficacy of our models we tested their performance against
520 the Bohn et al. [34] RNA-seq dataset which was not used to the train the models (Figure 6E). Here,
521 the performance on the trained Bru-seq and BruChase-seq data is reported as the five-fold cross-
522 validation performance for each of the 10 downsampled models. To observe the overall performance
523 of the models, we display precision-recall curves on both the Bru-seq and BruChase-seq data on
524 which the model was trained and the RNA-seq data for each of the 10 different models (Figure 6F).
525 The baseline is defined separately for each dataset as the overall class balance between the positive
526 and negative class. A perfect model tends toward the upper right of the graph, and a poor model
527 follows the dotted baseline for that dataset. Despite the differences in technique and biological
528 implications between RNA-seq and Bru-seq and BruChase-seq in determining PUM-mediated gene
529 regulation, we find that the models trained on Bru-seq and BruChase-seq are able to perform
530 well in predicting PUM-mediated regulation in RNA-seq data. We see similar performance when
531 considering a single definition for a PRE and only considering genes that have a least one PRE in
532 their 3' UTR (Figure S2A-D). Although the features we have included here are not sufficient to fully
533 describe PUM-mediated gene regulation in human cells, we have demonstrated a clear functional
534 association and predictive utility for PUM motifs (i.e. match scores and count of PREs) as well
535 as contextual features around PREs including the location, neighboring AU content, clustering of
536 PREs, and overlap with predicted miRNA sites.

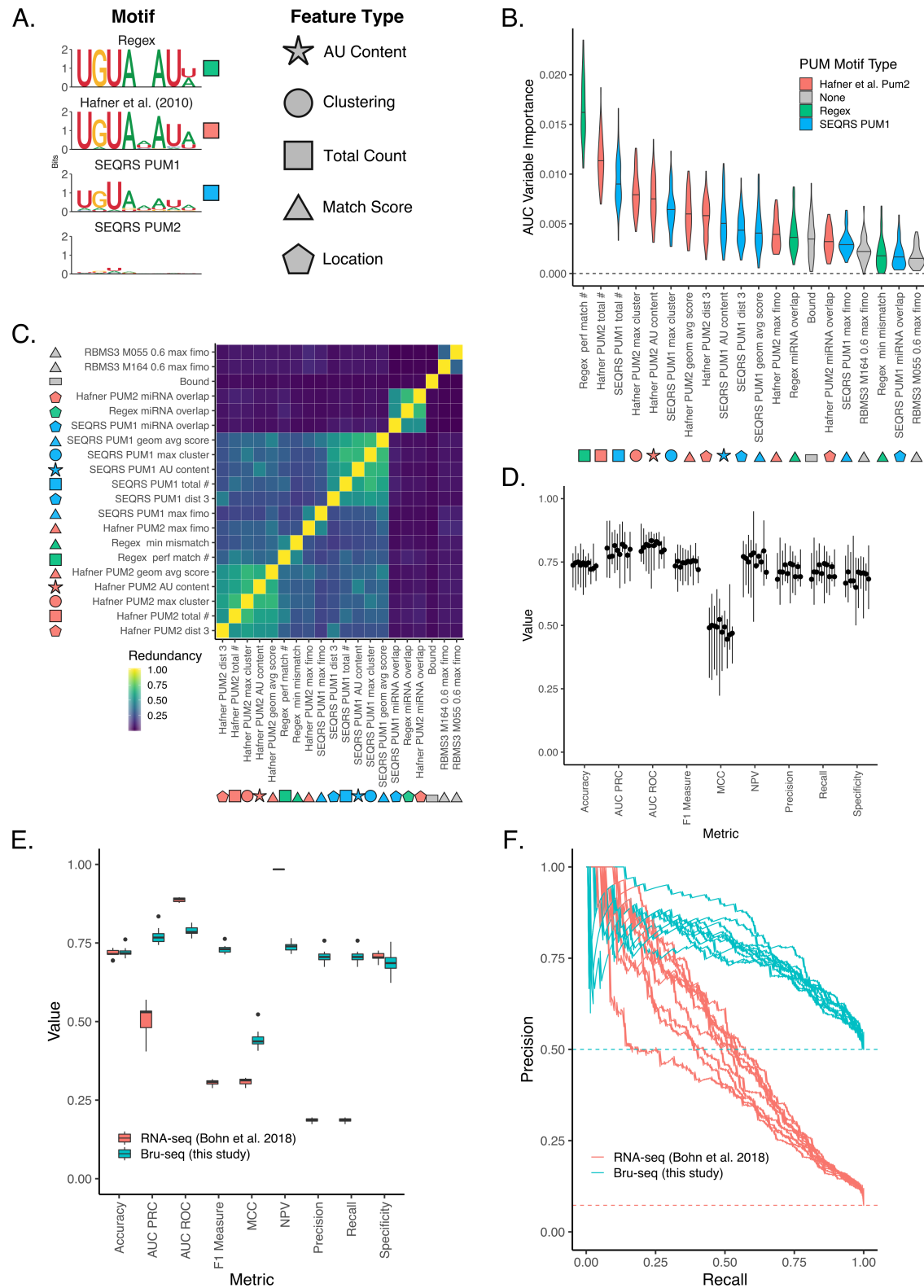


Figure 6 (*previous page*): Predicting PUM-mediated effect on decay using both sequence-based and experimental features. A) Motifs used to calculate features for machine learning. Shapes indicate the type of feature calculated, whereas colors indicate the motif used to calculate those features. Total count is a simple count of motifs; Match score refers to a numerical value indicating how well a sequence matches a motif; clustering indicates motif proximity to additional instances of the same motif; location indicates features associated with a single motif's location on the 3' UTR. Shapes filled in with the appropriate color are used to label features throughout the rest of the figure. B) Variable importance plot displaying the top twenty most important features, as determined by training a conditional random forest classifier on PUM decay data (see Methods for details including information on feature names). Violin plots represent density from ten separate downsamplings of the majority class, each with five fold cross-validation. An AUC based variable importance measure is used as described in Janitz et al. [78]. C) Calculation of the redundancy in information between the top twenty most important variables, as determined in A. Redundancy is calculated in the information-theoretic sense (see Methods for details) where 1 is completely redundant information and 0 is no redundancy in information between the two variables. D) Cross-validation of conditional random forest classifier performance. Each boxplot represents a separate downsample of the majority, no PUM-mediated effect class. Values for each boxplot represent the performance metric as calculated for each of five folds using a classification cutoff of 0.5. E) Performance of conditional random forest models on the steady state RNA data-set from [34]. Blue boxplots represent values from separate downsamplings of the majority, no PUM-mediated effect class used to train the model on the Bru-seq and BruChase-seq data set. Red boxplots indicate values from testing each model on the Bohn et al. [34] steady-state RNA-seq data set. Metrics were calculated using a classification cutoff of 0.5. F) Precision Recall curves using the models in E. Each line represents one of ten conditional random forest models trained on separate downsampled sets of the entire Bru-seq and BruChase-seq data set and tested on the steady state RNA data set.

537 **3. Discussion**

538 Through the combination of our high-throughput probing of RNA decay and the mining of
539 sequence information in the 3' UTRs of human transcripts, we were able to establish several general
540 rules of PUM-mediated gene regulation in human cells.

541 **3.1. Human PUM proteins control gene expression by modulating RNA stability**

542 Previous studies have established that both PUM1 and PUM2 control the stability of individual
543 transcripts through recognition of a UGUANAU PRE [32]. Transcriptome-wide measurements in
544 PUM1 and PUM2 knockdown conditions have shown that hundreds of RNAs change in abundance,
545 as measured using RNA-seq [34]. However, measurements of RNA abundance using RNA-seq only
546 allow for determination of changes in steady-state RNA abundances and do not allow one to dif-
547 ferentiate effects from changes in RNA stability versus changes in transcription rates. Through the
548 use of metabolic labeling, we are able to differentiate the effects of knocking down both PUM1 and
549 PUM2 on transcription from the effects on RNA stability [39]. Our results indicate that perturbing
550 the expression of human PUM1 and PUM2 has a widespread effect on the mRNA stability of many
551 transcripts in HEK293 cells, but does not appear to perturb transcription rates in any meaningful
552 way, as measured by our system. Rather than determine full decay rate constants for each tran-
553 script, which would have required the use of additional time points throughout the chase period
554 of our experiment, we chose to determine relative changes in RNA stability using just two time
555 points. The measurements obtained from these experiments cannot be interpreted on an absolute
556 scale, but the rank order of stability measurements within the experiment is preserved, allowing
557 us to determine the relative effects of PUM knockdown between any two genes [48]. Consistent
558 with the changes in steady-state RNA levels determined under PUM knockdown conditions, we see
559 transcripts that are both destabilized and stabilized. As expected, the number of genes that are
560 stabilized under PUM knockdown is much higher than the number of genes that were destabilized,
561 which is consistent with PUM's role in reducing the expression levels of target genes likely through
562 the recruitment of the CCR4-NOT complex and subsequent destabilization of the transcript [32].

563 *3.2. General rules for predicting PUM-mediated activation remain elusive*

564 In contrast with the clear and robust effects of PUM on PUM-repressed transcripts, the mech-
565 anism for the rarer case of PUM-mediated stabilization remains unclear. Measurements using
566 luminescent reporter assays have shown activation of a subset of predicted PUM-activated tran-
567 scripts that is dependent on the presence of a PRE in the 3' UTR of the reporter [34]. Furthermore,
568 direct binding of PUM1 or PUM2 to PREs present in the *FOXP1* 3' UTR has been reported to
569 promote expression of the FOXP1 protein, an important regulator of the cell cycle in hematopoiet-
570 ic stem cells [29]. Conversely, when considering PAR-CLIP measurements of PUM2 occupancy at
571 PREs for only the transcripts that were destabilized under PUM knockdown, we find inconclusive
572 evidence for binding in targeted examples (Figure 4C,D) and an insufficient number of examples
573 to draw firm conclusions when considering the group as a whole separately from the stabilized
574 transcripts (data not shown). Furthermore, attempts to classify transcripts that were stabilized
575 in PUM knockdown from those that were destabilized using random forest models with identical
576 feature sets to those used in Figure 6 showed poor performance, possibly due to the small num-
577 ber of examples for transcripts that were destabilized under PUM knockdown. There is also the
578 possibility that the destabilization of the transcripts under PUM knockdown are indirect effects
579 mediated through another factor that PUM is either directly regulating or PUM is competing with
580 for binding. It is likely that the PUM-mediated activation of genes found through high-throughput
581 studies represent a combination of direct and indirect targets. However, despite the clear evidence
582 for direct PUM-mediated activation of some targets, general rules for predicting PUM-mediated
583 activation remain elusive and mechanistic insights into PUM-mediated activation of key targets
584 will require further study.

585 *3.3. PUM1 and PUM2 have shared sequence preferences*

586 Using SEQRS [53] on purified PUM-HDs for both PUM1 and PUM2, we find a strong preference
587 for the UGUANAUUA motif for PUM1 and, somewhat surprisingly, a much weaker preference for
588 this motif for PUM2. However, when considering the enrichment of all possible 8mers, we see that
589 the preferences for each PUM-HD are highly correlated with a larger magnitude in enrichment
590 for PUM1 PUM-HD compared to PUM2 PUM-HD. Our approach uses a random library of RNA
591 sequences to determine RNA binding preferences and our analysis of PUM1 qualitatively agrees
592 with previous *in vitro* approaches with randomized libraries [51]. However, using a curated library
593 of sequences based on mutations from the consensus UGUANAUUA motif, Jarmoskaite et al. [52]
594 created a thermodynamic model for PUM2 binding that considers the effects of non-consecutive
595 bases in target recognition, as opposed to our simpler model that only considers the frequency of
596 occurrence of consecutive bases in a fully randomized library. Using this model, they show that
597 PUM-HDs from both PUM1 and PUM2 share nearly identical sequence preferences, which is in
598 agreement with our strong correlation in enrichment between the two proteins.

599 When we considered the local sequence content and location of PREs, we found that PREs
600 tend to be located towards the 3' end of the 3' UTR and have high local AU content. We are
601 not the first to observe these properties, as Jiang et al. [60] also arrived to this conclusion by
602 comparing the locations of shuffled PREs. However, we instead considered the locations of PREs
603 in simulated sets of 3' UTRs that share similar trinucleotide content to that of the true set of 3'
604 UTRs and this strengthens the claim that PREs are enriched in these areas more than one would
605 expect by chance. Furthermore, we are able to connect these observations directly to functional
606 outputs, showing that PREs in transcripts that had a significant change in RNA stability under
607 PUM knockdown are closer to the 3' end of the 3' UTR and have higher flanking AU content,
608 suggesting a functional role for the location of PREs within the 3' UTR itself. The non-random

609 propensity of PREs to occur towards the 3' end of the 3' UTR is consistent with a model where
610 PUMs recruit the CCR4-NOT complex for deadenylation of target sequences.

611 *3.4. Human Pumilio proteins regulate genes involved in signaling pathways*

612 When looking at the classes of genes that are stabilized under PUM knockdown, we find that
613 many GO terms with evidence for direct repression by PUMs revolve around regulating signaling
614 pathways mediated by proteins including kinases (GO:0018105), GEFs (GO:0005085), and receptor
615 signaling (GO:0030177, GO:0048008). The role of mammalian Pumilio proteins in modulating
616 signaling through controlling mRNA levels has been well established. In human testes, PUM2
617 is thought to interact with DAZL proteins to regulate germ-line development and many GTP-
618 binding, receptor-associated, and GEF encoding-mRNAs are found among a list of targets that
619 co-immunoprecipitate with both proteins [17]. Similarly, PUM1 has been shown to be important in
620 mouse testis development through downregulation of many proteins involved in MAPK signaling
621 and ultimate activation of p53 [18]. In fact, it has been argued that an ancestral function of the
622 PUF family of proteins is to regulate the maintenance of stem cells and cells that behave in a stem
623 cell-like manner through the down-regulation of kinases involved in critical signaling pathways [1].
624 Many studies looking at mRNAs associated with PUM1 or PUM2 binding in mammalian cells
625 tend to find similar sets of GO terms overlapping with PUM bound targets. Early RIP-Chip
626 experiments with human PUM1 and PUM2 found that genes bound by both proteins belonged to
627 GO terms associated with the Ras pathway, MAPK kinase cascade, PDGF signaling pathway, WNT
628 signaling pathway, small GTPase-mediated signal transduction, and transcription factor activity,
629 among others [35, 36]. More recent iCLIP experiments in mouse brains have found that mouse
630 PUM1 and PUM2 bind transcripts for genes associated with WNT signaling, regulation of MAP
631 kinase activity, small GTPase-mediated signal transduction, and several categories related to neural
632 development [22]. Similarly, changes in steady-state RNA abundance under both human PUM1
633 and human PUM2 knockdown identified several similar classes of genes including WNT signaling,
634 GEF activity, NOTCH signaling, and PDGF signaling [34]. Each of the categories noted above is
635 consistent with identified biological roles for mammalian PUMs. For example, mice lacking PUM1
636 and PUM2 have impaired learning and memory, as well as decreased neural stem cell proliferation
637 and survival [22]. Further, human PUM1 haploinsufficiency is associated with developmental delay
638 and ataxia [31]. Likewise, PUM2-deficient mice are more prone to chemically-induced seizures and
639 have impaired nesting abilities [20], and mouse PUM2 regulates neuronal specification in cortical
640 neurogenesis [23]. Our work shows that genes in these GO categories are modulated at the level
641 of mRNA stability, likely through direct interaction of the human PUM proteins by recognition of
642 PREs in the 3' UTR of transcripts.

643 In many ways, post-transcriptional regulation of proteins involved in signaling cascades is an
644 ideal way to rapidly modulate those pathways. In contrast to the delay in time between the
645 control of mRNA synthesis and the resulting protein production involved in regulating a gene at
646 the transcriptional level, post-transcriptional regulation allows for a rapid dampening of expression
647 levels directly where protein synthesis is occurring. Furthermore, gene regulation in the cytosol
648 allows for the possibility of localized control of expression [79]. In fact, temporal and localized
649 control of gene expression—important for proper development of the fly embryo—was exactly how
650 the PUF family of proteins were initially discovered [13]. Given the emerging role for human
651 PUM proteins in neuronal development and function, and the need for localized control of gene
652 expression in neuronal tissue [80] it is conceivable that PUM proteins could be heavily involved in
653 RNA polarity within the neuron as has been observed in *C. elegans* olfactory neurons [81].

654 3.5. *Prediction of PUM-mediated regulation defines a set of general principles for an ideal PUM*
655 *target site*

656 Many attempts have been made to predict gene regulation by Pumilio proteins given sequence
657 information about the possible targets. Previously, a biologically inspired model based strictly on
658 the count of PREs within the 5' UTR, CDS, and 3' UTR was fit to steady state RNA levels [34].
659 In this model, the effects of having multiple PREs on a single transcript were found to be less
660 than linear on the target response to PUM knockdown, which was interpreted to indicate that
661 multiple PRE sites function to increase the odds of having a PUM bound and that a single PRE
662 likely performs most of the functions needed for PUM-mediated regulation [34]. In this study we
663 expanded the feature set of possible predictors for PUM-mediated activity and determine a set of
664 rules that define a functional PRE. Consistent with the Bohn et al. [34], we find that a simple count
665 of PREs in the 3' UTR acts as the best predictor for PUM activity. However, surprisingly we find
666 that the simple UGUA.AU[AU] regular expression outperforms more sophisticated PWM-based
667 definitions from either *in vivo* and *in vitro* high throughput data. This may indicate that, although
668 PUMs can bind PREs with mismatches from this consensus motif, the UGUANAUA may represent
669 the “ideal” PRE for functional regulation. In fact, structural studies of human PUM1 and PUM2
670 have identified three different modes of binding between the nucleotide bases of the fifth base in the
671 consensus motif and the amino acids of PUM repeats 4 and 5. Lu and Hall [82] show that changes
672 between these modes of binding do not alter PUM binding affinity, but could conceivably present
673 different surfaces for effector proteins. Although our regular expression allows for any base at the
674 fifth position, PUM repeats are modular [7] and it is conceivable that a similar mechanism could
675 apply to other bases in the motif. Additionally this suggests that PUM binding to the UGUANAUA
676 consensus motif could represent the ideal structure for PUMs interaction with effector molecules.
677 We also find sequence features surrounding a PRE to be important in predicting PUM activity
678 on a target. High AU content and position within the 3' UTR both appear to be important for
679 predicting mammalian PUM regulation. Consistent with prior reports of cooperativity between
680 PUM and miRNAs [36, 50, 60, 65], we find that a count of predicted miRNA sites near PREs
681 helps predict PUM effect, with a higher number of miRNA sites near a PRE indicating a larger
682 stabilization under PUM knockdown (Figure S1A). It is possible that PUM could act to block or
683 enhance miRNA function through direct interactions with the miRNA machinery or through local
684 rearrangements of RNA secondary structure.

685 Secondary structure has been predicted to have an effect on many RBPs [51] and PUM has been
686 shown to change secondary structure upon binding to facilitate miRNA interaction [65]. However,
687 we found that *in silico* predictions of RNA secondary structure around PREs were not predictive
688 of PUM function (Figure S1C). Targeted regression models considering PRE count and structure
689 performed worse when structural information was added (data not shown). Recent studies have
690 shown that structural probing experiments used in tandem with *in silico* folding algorithms vastly
691 improve biological predictions based on structural information [83]. Similar methods may be needed
692 to determine the role of secondary structure in PUM-mediated regulation. Alternatively, PUM
693 proteins may be able to overcome RNA secondary structure in order to bind PREs, in which case,
694 secondary structure would have no bearing on PUM binding. Similarly, RNA modifications may
695 limit the ability for PUM to recognize PREs. Recent efforts have identified m6A sites across the
696 human transcriptome at single nucleotide resolution [84]; however, we find limited to no overlap
697 between m6A sites and PREs (data not shown).

698 There has also been a recent interest in the role of codon optimality in mRNA decay in human
699 cells [85, 86]. Using, as a measure of codon optimality, the fraction of optimal codons—where
700 a codon is designated as optimal if its Codon Stability Coefficient is positive [87]—we find that
701 PUM targets undergoing PUM-mediated decay in our data set have a lower fraction of optimal

702 codons on average than those with no PUM-mediated effect (Figure S1B). However, the fraction of
703 optimal codons did not rank in the top twenty most important features for differentiating between
704 transcripts subject to PUM-mediated decay from those that are not affected in our machine learning
705 models (Figure 6). Recent studies have implicated codon optimality as an important determinant
706 of mRNA stability in eukaryotes [85–88] and it is conceivable that PUM proteins could be directly
707 mediating some of these effects. However, it is also possible that RNAs with a lower fraction of
708 optimal codons represent more ideal targets for PUM or that PUM could be interacting with the
709 factors that mediate decay for RNAs with less optimal codons. Further studies will be needed to
710 establish the relationship between PUM and codon optimality.

711 By combining high-throughput functional data with statistical modeling, we have identified
712 several contextual features around PREs that have improved our understanding of PUM-mediated
713 gene regulation and increased our ability to predict PUM targets. However, there is still substan-
714 tial room for improvement. Recent successes in Pumilio target prediction in *Drosophila* have come
715 from characterizing binding partners of DmPum: Nos and Brat [89]. Nos binds together with
716 DmPum to modulate the 5' sequence specificity of the Pum-Nos complex, thus introducing fine-
717 tune control over Pum target recognition [11]. A recent study identified many new and previously
718 known interacting partners for the human PUM1 and PUM2 proteins including DAZL, PABP,
719 FMRP, miRISC, and members of the CCR4-NOT complex [90]. Like the Nos/DmPum example,
720 these partners likely add an additional layer of information in the control of PUM-mediated gene
721 regulation. Furthermore, the probing of RNA secondary structure *in vivo* may allow for better in-
722 corporation of secondary structural information into models of PUM-mediated regulation. Finally,
723 we were unable to find determinants of PUM-mediated activation, an area that is rich for future
724 targeted experiments.

725 4. Materials and Methods

726 4.1. Experimental methodology

727 4.1.1. SEQR S protein purification

728 Methods are reproduced here from Weidmann et al. [11]. Recombinant Halo-tag PUM1 RBD (aa
729 828-1176) and Halo-tag PUM2 RBD (aa 705-1050) were expressed from plasmid pFN18A (Promega)
730 in KRX *E. coli* cells (Promega) in 2xYT media with 25 μ g/mL kanamycin and 2mM MgSO₄ at 37°C
731 to OD₆₀₀ of 0.7–0.9, at which point protein expression was induced with 0.1% (w/v) rhamnose for
732 3hr. The PUM RBD expression constructs were originally described in Van Etten et al. [32]. Cell
733 pellets were washed with 50mM Tris-HCl, pH 8.0, 10% (w/v) sucrose and pelleted again. Pellets
734 were suspended in 25mL of 50mM Tris-HCl pH 8.0, 0.5mM EDTA, 2mM MgCl₂, 150mM NaCl,
735 1mM DTT, 0.05% (v/v) Igepal CA-630, 1mM PMSF, 10 μ g/ml aprotinin, 10 μ g/ml pepstatin,
736 and 10 μ g/ml leupeptin. To lyse cells, lysozyme was added to a final concentration of 0.5 mg/mL
737 and cells were incubated at 4°C for 30min with gentle rocking. MgCl₂ was increased to 7mM and
738 DNase I (Roche) was added to 10 μ g/mL, followed by incubation for 20 min. Lysates were cleared
739 at 50,000 $\times g$ for 30min at 4°C. Halo-tag containing proteins were purified using Magnetic HaloLink
740 Resin (Promega) at 4°C. Beads were washed 3 times with 50mM Tris-HCl pH 8.0, 0.5mM EDTA,
741 2mM MgCl₂, 1M NaCl, 1mM DTT, 0.5% [v/v] Igepal CA-630) and 3 times with Elution Buffer
742 (50mM Tris-HCl, pH 7.6, 150mM NaCl, 1mM DTT, 20% [v/v] glycerol).

743 To confirm protein expression, beads were resuspended in Elution Buffer with 30 U of AcTEV
744 protease (Invitrogen), cleavage proceeded for 24hr at 4°C, and beads were removed by centrifugation
745 through a micro-spin column (Bio-Rad). Concentration of eluted protein was measured by Bradford
746 assay, followed by coomassie stained SDS-PAGE analysis.

747 SEQRS was conducted on PUM1 PUM-HD and PUM2 PUM-HD as described in Campbell
748 et al. [9] with minor modifications including the use of Magnetic Halolink beads (Promega). The
749 PUM test proteins remained covalently bound via N-terminal Halotag to the beads.

750 The initial RNA library was transcribed from 1 μ g of input dsDNA using the AmpliScribe T7-
751 Flash Transcription Kit (Epicentre). 200 ng of DNase treated RNA library was added to 100 nM
752 of Halo-tagged proteins immobilized onto magnetic resin (Promega). The volume of each binding
753 reaction was 100 μ l in SEQRS buffer containing 200 ng yeast tRNA competitor and 0.1 units of
754 RNase inhibitor (Promega). The samples were incubated for 30min at 22°C prior to magnetic
755 capture of the protein-RNA complex. The binding reaction was aspirated and the beads were
756 washed four times with 200 μ l of ice cold SEQRS buffer. After the final wash step, resin was
757 suspended in elution buffer (1mM Tris pH 8.0) containing 10 pmol of the reverse transcription
758 primer. Samples were heated to 65°C for 10min and then cooled on ice. A 5 μ l aliquot of the
759 sample was added to a 10 μ l ImProm-II reverse transcription reaction (Promega). The ssDNA
760 product was used as a template for 25 cycles of PCR using a 50 μ l GoTaq reaction (Promega).

761 *4.1.2. Bru-seq and BruChase-seq experimental procedure*

762 Bru-seq and BruChase-seq were conducted as described in Paulsen et al. [39] in HEK293 cells
763 grown in the presence of siPUM1/2 or siNTC. RNAi conditions and siRNA sequences were previ-
764 ously described by Bohn et al. [34] and include treatment with siRNAs for 48hrs to allow for PUM
765 depletion prior for BrU labeling. Four replicates were gathered for each time point and siRNA con-
766 dition, resulting in 16 total samples. Resulting cDNA libraries were sequenced using an Illumina
767 HiSeq 2000 via the University of Michigan Sequencing core.

768 *4.2. Bru-seq and BruChase-seq Computational analysis*

769 *4.2.1. Modeling PUM-mediated RNA decay*

770 Sequencing reads were aligned to the human genome (hg19) and processed according to Paulsen
771 et al. [39] up to obtaining read counts for exons and introns for each gene and sample. Our
772 experimental design resulted in four different replicates of siNTC (WT) and siPUM1/2 (PUMKD)
773 conditions with two different time points each: t_{0hr} and t_{6hr} . For the t_{0hr} time points, read counts
774 from both exons and introns were pooled for each gene. For the t_{6hr} time points, only read counts
775 from exons were used. Read abundance was modeled using DESeq2 [49]. As described in Love
776 et al. [49], DESeq2 models read count abundance K for gene i in sample j using the generalized
777 linear model described below:

$$K_{ij} \sim NB(\mu_{ij}, \alpha_i) \quad (1)$$

778 Where α_i is a gene-specific dispersion parameter for gene i and μ_{ij} is defined by the following:

$$\mu_{ij} = s_j q_{ij} \quad (2)$$

779 Here, s_j is a sample specific size factor used to put read count abundances on the same scale
780 between samples. Finally, $q_{i,j}$ is defined according to our design matrix:

$$\log_2(q_{i,j}) = \beta_0 + \beta_c c + \beta_t t + \beta_{tc} t c \quad (3)$$

781 Where, c is an indicator variable that is 0 when the sample is in condition WT and 1 when
782 the sample is in condition PUMKD. Likewise, t is an indicator variable that is 0 when sample is
783 in the 0 hour time point and 1 when the sample is in the 6 hour time point. We interpret the
784 β_{tc} term to represent changes in RNA stability resulting specifically from the PUM KD condition.

785 Similarly we interpret the β_c term to represent changes in transcription rates between the two
786 conditions. Throughout the text, unless otherwise noted, we report β_{tc} normalized by the reported
787 standard error for the coefficient, which amounts to the Wald statistic computed for that term by
788 DESeq2. Thus, the Wald statistic for the interaction term is denoted as “RNA stability in PUM
789 KD” throughout the text and is a unitless quantity.

790 *4.2.2. Analysis of transcriptional vs. stability effects*

791 To test for significant changes in transcription or stability, the Wald test statistic for the ap-
792 propriate term— β_c for transcription and β_{tc} for stability—was calculated as described above. The
793 Wald statistic was compared to a zero centered normal distribution and a two-tailed p-value was
794 calculated using statistical programming language R’s `pnorm` function (n.b. this is virtually equiv-
795 alent to the p-values calculated by the DEseq2 package for contrasts [49]). To test for a statistically
796 significant lack of change in transcription or stability, the Wald statistic for the appropriate term
797 was compared to a normal distribution centered at the nearest boundary of a region of practical
798 equivalence (ROPE) and a two-tailed p-value was calculated using R’s `pnorm` function. The ROPE
799 was defined as $\log_2(1/1.75) - \log_2(1.75)$ and was chosen to be within the range of fold expression
800 change of a RnLuc reporter gene with between one and three PREs in its minimal 3’ UTR [34].
801 Each p-value was FDR-corrected using the Benjamini-Hochberg procedure [91] and, for each term,
802 the smaller of the two FDR-corrected p-values was reported. In order for a gene to be classified
803 in the EFFECT class the following conditions had to be met: 1. its change in stability q-value
804 had to be smaller than its no change in stability q-value; 2. Its change in stability q-value had to
805 pass a cutoff of 0.05 for statistical significance; and 3. The original \log_2 fold-change value had to
806 be outside the defined ROPE. In contrast, in order for a gene to be classified in the NOEFFECT
807 class the following conditions had to be met: 1. it was not classified as an EFFECT gene; 2. its no
808 change in stability q-value had to be smaller than its change in stability q-value; 3. its no change
809 in stability q-value had to pass a cutoff of 0.05 for statistical significance; and 4. The original \log_2
810 fold-change value had to be within the defined ROPE. Genes not passing the criteria for either the
811 EFFECT or NOEFFECT groups are those for which we lack sufficient information to make any
812 strong statement on the effects of PUM knockdown.

813 *4.3. SEQRS Computational analysis*

814 Each raw sequencing read from the SEQRS experiments has the following expected structure:
815 NNNNNN-CTGATCCTACCATCCGTGCT-NNNNNNNNNNNNNNNNNN-CACAGCTT
816 CGTACCGAGCGG-GATCGGAAGA-XXXXXX-ATCTCGTA

817 Where X represents a known barcode sequence used to split the reads from a multiplexed
818 experiment and N represents a random variable base. The *in vitro* transcription reaction uses
819 the above sequence as a template resulting in RNA with sequence starting from the 3’ end of the
820 CACAGCTTCGTACCGAGCGG downstream of the 20mer and going in the opposite direction.
821 Thus, the RNA molecules in the SEQRS experiments are the reverse complement of the following:
822 CTGATCCTACCATCCGTGCT-NNNNNNNNNNNNNNNNNN-CACAGCTTCGTACC
823 GAGCGG

824 Raw sequencing reads were split by barcode, allowing for up to two pairwise mismatches on
825 both the upstream and downstream adapter sequences. The 20mer variable regions and constant
826 flanking adapter sequences of each read were reverse complemented and broken into all possible
827 8mer sequences using a sliding window, and raw counts for all possible 8mer abundances for each
828 sequencing round for each protein were calculated using custom python scripts. For 8mers that
829 overlapped the constant flanking adapter sequences, only 8mers that had at least one base in the
830 variable region were considered.

831 To determine position-weight matrices that best represented selection by the protein of interest
832 for that round, we followed the approach of Jolma et al. [57] in the analysis of DNA-binding proteins
833 using SELEX. Briefly, a seed sequence is determined from the most abundant N-mer within that
834 round. From this seed sequence, the abundance of each base at a given position was tallied when all
835 other positions match the seed sequence. The PWM frequencies were determined by dividing each
836 column of the resulting count matrix by its column sum. For all PWMs determined by this method
837 we used a UGUAAAUA seed sequence. Unlike Jolma et al. [57] we do not include the correction
838 for non-specific carryover of nucleic acid from the previous cycle as the assumption that no more
839 than 25% of 8mers would be expected to be bound may not hold for RNA-binding proteins due to
840 their promiscuous binding [51]. Instead, we accounted for the bias of the initial sequencing pool by
841 calculating a PWM for the initial pool using the UGUAAAUA seed sequence. We then divided the
842 position frequency matrix of each PWM by the initial sequencing pool's position frequency matrix.
843 Finally, we determined the bias-corrected frequency matrix by dividing each column of the matrix
844 by its column sum.

845 In order to compare 8mer selection between rounds or proteins, the enrichment of a particular
846 8mer was calculated with the following equation:

$$E = \log_2 \left(\frac{\frac{c_{s,i}}{\sum_{i=1}^{N_s} c_{s,i}}}{\frac{c_{b,i}}{\sum_{i=1}^{N_b} c_{b,i}}} \right) \quad (4)$$

847 Where $c_{s,i}$ represents the count for 8mer i in sample s and $c_{b,i}$ represents the count for 8mer i in
848 blank round where the input sequences were sampled. The DmPum data and corresponding blank
849 sample was accessed from Weidmann et al. [11] and only the first five rounds were considered.

850 4.4. GO term analysis and iPAGE

851 GO term analysis was performed using the integrative pathway analysis of gene expression
852 (iPAGE) software package [70]. Genes were discretized by the interaction term Wald test statistic
853 into five-equally populated bins and iPAGE was run with default settings.

854 4.5. Determination of matching PREs

855 The full set of 3' UTRs for hg19 genome was downloaded using the TxDb.Hsapiens.UCSC.-
856 hg19.knownGene, BSgenome.Hsapiens.UCSC.hg19, and GenomicFeatures R packages. Matches
857 to a given PWM across all 3' UTRs were determined using the FIMO package with a uniform
858 background using default cutoffs for reporting matches [92]. For PRE-centric figures, such as the
859 heatmaps and violin plots in Figure 3 and Figure S1, each unique 3' UTR isoform is matched to
860 its corresponding "RNA stability in PUM KD" value by gene name, and each feature's value is
861 reported as the given summary statistic over a given 3' UTR isoform for that feature, as described
862 in the section below (i.e., for AU content, the value reported is the maximum AU content around
863 any given PRE within that 3' UTR isoform).

864 For *de novo* discovery of informative motifs in our Bru-seq and BruChase-seq dataset, we
865 applied the finding informative regulatory elements (FIRE) software [59] with default settings to
866 each unique 3' UTR isoform matched to its "RNA stability in PUM KD" value and discretized into
867 ten equally populated bins.

868 To calculate the location and AU content of PREs in randomly generated sets of the 3' UTRs,
869 a third order Markov model was trained on the annotated set of unique 3' UTR isoforms from
870 the hg19 genome. One thousand randomly simulated sets of 3' UTRs—each with the same length
871 as the annotated set of 3' UTRs—was then generated using custom python scripts. For each of

872 the thousand simulated sets of 3' UTRs, the fifth round SEQRS PUM1 (Figure 2A) was used to
873 search for matches using FIMO as described above. Here each individual PRE was considered in
874 the calculation of the kernel density plots shown in Figure 3.

875 To determine the PAR-CLIP read coverage at identified PRE sites in the set of known unique
876 3' UTR isoforms, raw reads were downloaded from SRA with accession numbers SRR048967 and
877 SRR048968. Raw fastq files were processed with trimmomatic [93] and cutadapt [94] to remove
878 low quality reads and illumina adapters. Processed reads were aligned to the hg19 genome using
879 the STAR aligner with default parameters [95]. Read coverage and T to C mutations were deter-
880 mined for reads within 20 bp of each PRE in each unique 3' UTR isoform for both EFFECT and
881 NOEFFECT genes, individually, using custom python scripts. Coverage over all PREs was aligned
882 and the bottom and top 5% of read coverage at each position was removed from the average cal-
883 culation. Error bars were determined by bootstrapping, with stratified sampling with replacement
884 read coverage from individual PREs in each group separately.

885 4.6. *Determination of PRE clustering*

886 To determine whether the PREs cluster together more than would be expected by chance, we
887 determined the ratio of the observed frequency of PUM sites within all possible 100 bp windows
888 of 3' UTRs with a least 1 PRE in them to a Poisson model with the rate parameter, λ , set to the
889 average count of PREs within all 100 bp windows. 95% confidence intervals were determined by
890 bootstrapping the observed distribution of PRE counts within all windows.

891 4.7. *Predicting PUM-mediated regulation using conditional random forest models*

892 In order to predict the PUM-mediated regulation on a given transcript, we used conditional
893 random forest models as implemented by the cforest function from the party R package [96–98].
894 Binary classification models were trained using default settings with no parameter tuning on the
895 Bru-Seq EFFECT and NOEFFECT classes and a permutation-based AUC variable importance
896 metric was calculated for each individual model [78]. Due to the large class imbalance, ten separate
897 datasets were generated from the full dataset, where the majority NOEFFECT class was randomly
898 downsampled to match the EFFECT class. Within each of the ten datasets, five-fold cross validation
899 was performed to assess performance and detect overtraining. Final models were generated using
900 the ten downsampled datasets without cross-validation and performance was tested on the RNA-
901 seq dataset from Bohn et al. [34]. Precision-recall plots were calculated using the PRROC package
902 based on the methodology of Davis and Goadrich [99].

903 4.7.1. *Calculation of features associated with a PWM*

904 For each of the features described, the values were first calculated individually for each unique
905 3' UTR isoform. Values for each isoform were combined by taking the mean of the value for that
906 feature and isoform weighted by the number of isoforms that shared that unique 3' UTR in the full
907 set of annotated 3' UTRs in the hg19 genome. For features ending in “fimo_best_bygene_max_fimo”,
908 the maximum FIMO match score for each unique 3' UTR isoform for that PWM was calculated
909 by setting the p-value cutoff threshold in FIMO to 1.1, thereby allowing FIMO to consider every
910 possible match for a given sequence. The maximum match score for each sequence was reported
911 for each unique 3' UTR isoform. For features ending in “fimo_best_bygene_total_num”, the total
912 number of matching sites for a given unique 3' UTR isoform was calculated as described above in
913 the “Determination of matching PREs” section. For each sequence, the geometric average of FIMO
914 scores for each matching PRE was calculated and reported in the “fimo_bygene_geom_avg_score”.
915 The maximum match score, geometric average match score, and total match number was calculated

916 for the SEQRS PUM1 round 5 PWM, SEQRS PUM2 round 5 PWM, Hafner et al. [37] PUM2 PWM,
917 and each of the PWMs for human RBPs found in the CISBP-RNA database [100].

918 For PREs, the shortest distance to the 3' UTR for any given PRE is converted to normalized co-
919 ordinates (i.e., 0.0 is the 5' end and 1.0 is the 3' end) and reported in the “fimo_best_bygene_dist_3’”.
920 For “fimo_bygene_at_content” the largest percentage AT content in a 100 bp window surrounding
921 any PRE within a given sequence was reported. Similarly for “fimo_bygene_max_cluster”, the max-
922 imum number of full PRE sites within a sliding of 100 bp was calculated. For both of these features,
923 windows were truncated at the 3' and 5' ends of the sequence.

924 Predicted miRNA sites were determined using default predictions (conserved sites of conserved
925 miRNA families) from TargetScan release 7.2 [67]. Overlaps with PREs were calculated by counting
926 miRNA sites within a 100 bp window surrounding each PRE. For 3' UTRs with more than one
927 PRE, the PRE with the maximum number of overlapping miRNA sites was considered.

928 4.7.2. Calculation of *in silico* basepairing probabilities for PREs

929 For each identified PRE, the probability of the given PRE being base-paired within predicted
930 secondary structure was calculated using RNAfold [101] by calculating the ensemble free energy of
931 an unconstrained sequence F_u of 50 bp flanking each side of a given PRE and the ensemble free
932 energy of a constrained sequence where no base within the PRE is allowed to form a base pair F_c .
933 The probability of the PRE being constrained from base-pairing can be calculated using:

$$P_c = \exp\left(\frac{(F_u - F_c)}{RT}\right) \quad (5)$$

934 Where T is the temperature (set to physiological temperature, 310.15K), and R is the gas
935 constant (set to 0.00198 kcal K⁻¹ mol⁻¹). Thus the probability of any given PRE being un-
936 paired is P_c . We define two features associated with P_c for each PRE in a given 3' UTR isoform.
937 “avgprob_unpaired” is the average P_c of all the PREs within a given 3' UTR and “maxprob_unpaired”
938 is the maximum P_c of all the PREs within a given 3' UTR. Values for each isoform were combined
939 into gene level estimates, as described above.

940 4.7.3. Calculation of information redundancy between features

941 In order to calculate the information redundancy between features, each feature was discretized
942 into ten equally populated bins. The redundancy between feature 1 (F_1) and feature 2 (F_2) was
943 calculated with the following equation:

$$R = \frac{2 \times I(F_1; F_2)}{(H(F_1) + H(F_2))} \quad (6)$$

944 Where H is the entropy of a given vector X of discrete values, as defined below:

$$H(X) = - \sum_{x \in X} P(x) \log_2(P(x)) \quad (7)$$

945 And the mutual information $I(X; Y)$ of vectors X and Y of discrete values is defined as:

$$I(X; Y) = \sum_{x \in X} \sum_{y \in Y} P(x, y) \log\left(\frac{P(x, y)}{P(x)P(y)}\right) \quad (8)$$

946 4.7.4. *Determination of EFFECT and NOEFFECT classes for RNA-seq data*

947 RNA-seq data was obtained from Bohn et al. [34] and a gene was only considered if the FPKM for
948 both the PUM1/2 knockdown condition and the siNTC condition were greater than 5. Genes that
949 passed this cutoff and that were considered to have statistically significant differential expression
950 in the original analysis were considered EFFECT genes. Genes that passed the cutoff and were
951 not considered to have statistically significant differential expression were considered NOEFFECT
952 genes.

953 5. Acknowledgments

954 This work was supported in part by the National Institute of General Medical Sciences, Na-
955 tional Institutes of Health grant R35 GM128637 to P.L.F. and grant R01 GM105707 to A.C.G..
956 Additionally, this work was supported by National Institute of Neurological Disorders and Stroke,
957 Grant/Award Number: R01NS100788 and NIH Grant/Award Number: 1UG3TR003149 to Z.T.C.
958 as well as NIH Grant/Award Number: UM1 HG009382 and NIH Grant/Award Number: R01
959 CA213214 01 to M.L.. Work by M.B.W. was supported by the National Science Foundation Grad-
960 uate Research Fellowship DGE1256260. Work by B.M. was supported by the NCI through the
961 Rogel Cancer Center support grant P30CA046592.

962 5.1. Author contributions

963 Bioinformatics/computational analysis: Michael Wolfe (Data analysis and primary manuscript
964 author), Peter Freddolino (Funding and concept, data analysis, writing); Bru-seq and BruChase-seq:
965 Trista Schagat (RNAi, RNA labeling and purification), Aaron Goldstrohm (Funding and Concept,
966 writing), Michelle Paulsen (Bru RNA Seq), Brian Magnuson (initial Bru-seq and BruChase-seq
967 data analysis), Mats Ljungman (Funding and concept); PUM Protein Purification for SEQRS:
968 Daeyoon Park, Chi Zhang and Zak Campbell (SEQRS and data analysis, funding)

969 6. References

- 970 [1] Marvin Wickens, David S. Bernstein, Judith Kimble, and Roy Parker. A PUF family portrait:
971 3'UTR regulation as a way of life. *Trends in Genetics*, 18(3):150–157, March 2002. ISSN
972 0168-9525. doi: 10.1016/S0168-9525(01)02616-6.
- 973 [2] Stefanie Jonas and Elisa Izaurralde. Towards a molecular understanding of microRNA-
974 mediated gene silencing. *Nature Reviews Genetics*, 16(7):421–433, July 2015. ISSN 1471-0056.
975 doi: 10.1038/nrg3965.
- 976 [3] Stefanie Gerstberger, Markus Hafner, and Thomas Tuschl. A census of human RNA-binding
977 proteins. *Nature Reviews Genetics*, 15(12):829–845, December 2014. ISSN 1471-0056. doi:
978 10.1038/nrg3813.
- 979 [4] Melanie A. Miller and Wendy M. Olivas. Roles of Puf proteins in mRNA degradation and
980 translation. *WIREs RNA*, 2(4):471–492, 2011. ISSN 1757-7012. doi: 10.1002/wrna.69.
- 981 [5] Aaron C. Goldstrohm, Traci M. Tanaka Hall, and Katherine M. McKenney. Post-
982 transcriptional Regulatory Functions of Mammalian Pumilio Proteins. *Trends in Genetics*,
983 34(12):972–990, December 2018. ISSN 0168-9525. doi: 10.1016/j.tig.2018.09.006.

984 [6] Xiaoqiang Wang, Phillip D. Zamore, and Traci M. Tanaka Hall. Crystal Structure of a
985 Pumilio Homology Domain. *Molecular Cell*, 7(4):855–865, April 2001. ISSN 1097-2765. doi:
986 10.1016/S1097-2765(01)00229-5.

987 [7] Xiaoqiang Wang, Juanita McLachlan, Phillip D. Zamore, and Traci M. Tanaka Hall. Modular
988 Recognition of RNA by a Human Pumilio-Homology Domain. *Cell*, 110(4):501–512, August
989 2002. ISSN 0092-8674. doi: 10.1016/S0092-8674(02)00873-5.

990 [8] Shuyun Dong, Yang Wang, Caleb Cassidy-Amstutz, Gang Lu, Rebecca Bigler, Mark R.
991 Jezyk, Chunhua Li, Traci M. Tanaka Hall, and Zefeng Wang. Specific and Modular Binding
992 Code for Cytosine Recognition in Pumilio/FBF (PUF) RNA-binding Domains. *Journal of
993 Biological Chemistry*, 286(30):26732–26742, July 2011. ISSN 0021-9258, 1083-351X. doi:
994 10.1074/jbc.M111.244889.

995 [9] Zachary T. Campbell, Cary T. Valley, and Marvin Wickens. A protein-RNA specificity
996 code enables targeted activation of an endogenous human transcript. *Nature Structural &
997 Molecular Biology*, 21(8):732–738, August 2014. ISSN 1545-9985. doi: 10.1038/nsmb.2847.

998 [10] Zachary T. Campbell, Devesh Bhimsaria, Cary T. Valley, Jose A. Rodriguez-Martinez, Elena
999 Menichelli, James R. Williamson, Aseem Z. Ansari, and Marvin Wickens. Cooperativity in
1000 RNA-Protein Interactions: Global Analysis of RNA Binding Specificity. *Cell Reports*, 1(5):
1001 570–581, May 2012. ISSN 2211-1247. doi: 10.1016/j.celrep.2012.04.003.

1002 [11] Chase A. Weidmann, Chen Qiu, René M. Arvola, Tzu-Fang Lou, Jordan Killingsworth,
1003 Zachary T. Campbell, Traci M. Tanaka Hall, and Aaron C. Goldstrohm. Drosophila Nanos
1004 acts as a molecular clamp that modulates the RNA-binding and repression activities of
1005 Pumilio. *eLife*, 5:e17096, August 2016. ISSN 2050-084X. doi: 10.7554/eLife.17096.

1006 [12] Chen Qiu, Vandita D. Bhat, Sanjana Rajeev, Chi Zhang, Alexa E. Lasley, Robert N. Wine,
1007 Zachary T. Campbell, and Traci M. T. Tanaka Hall. A crystal structure of a collaborative
1008 RNA regulatory complex reveals mechanisms to refine target specificity. *eLife*, August 2019.
1009 doi: 10.7554/eLife.48968.

1010 [13] Ruth Lehmann and Christiane Nüsslein-Volhard. Involvement of the pumilio gene in the
1011 transport of an abdominal signal in the Drosophila embryo. *Nature*, 329(6135):167, September
1012 1987. ISSN 1476-4687. doi: 10.1038/329167a0.

1013 [14] Robin P. Wharton and Gary Struhl. RNA regulatory elements mediate control of Drosophila
1014 body pattern by the posterior morphogen nanos. *Cell*, 67(5):955–967, November 1991. ISSN
1015 0092-8674. doi: 10.1016/0092-8674(91)90368-9.

1016 [15] P D Zamore, J R Williamson, and R Lehmann. The Pumilio protein binds RNA through a
1017 conserved domain that defines a new class of RNA-binding proteins. *RNA*, 3(12):1421–1433,
1018 December 1997. ISSN 1355-8382.

1019 [16] Danislav S. Spassov and Roland Jurecic. Cloning and comparative sequence analysis of PUM1
1020 and PUM2 genes, human members of the Pumilio family of RNA-binding proteins. *Gene*,
1021 299(1):195–204, October 2002. ISSN 0378-1119. doi: 10.1016/S0378-1119(02)01060-0.

1022 [17] Mark Fox, Jun Urano, and Renee A. Reijo Pera. Identification and characterization of RNA
1023 sequences to which human PUMILIO-2 (PUM2) and deleted in Azoospermia-like (DAZL)
1024 bind. *Genomics*, 85(1):92–105, January 2005. ISSN 0888-7543. doi: 10.1016/j.ygeno.2004.10.
1025 003.

1026 [18] Dong Chen, Wei Zheng, Aiping Lin, Katherine Uyhazi, Hongyu Zhao, and Haifan Lin. Pumilio
1027 1 Suppresses Multiple Activators of p53 to Safeguard Spermatogenesis. *Current Biology*, 22
1028 (5):420–425, March 2012. ISSN 0960-9822. doi: 10.1016/j.cub.2012.01.039.

1029 [19] John P. Vessey, Lucia Schoderboeck, Ewald Gingl, Ettore Luzi, Julia Riefler, Francesca Di
1030 Leva, Daniela Karra, Sabine Thomas, Michael A. Kiebler, and Paolo Macchi. Mammalian
1031 Pumilio 2 regulates dendrite morphogenesis and synaptic function. *Proceedings of the National
1032 Academy of Sciences*, 107(7):3222–3227, February 2010. ISSN 0027-8424, 1091-6490. doi:
1033 10.1073/pnas.0907128107.

1034 [20] Henrike Siemen, Damien Colas, H. Craig Heller, Oliver Brüstle, and Renee A. Reijo Pera.
1035 Pumilio-2 Function in the Mouse Nervous System. *PLOS ONE*, 6(10):e25932, October 2011.
1036 ISSN 1932-6203. doi: 10.1371/journal.pone.0025932.

1037 [21] Vincenzo A. Gennarino, Ravi K. Singh, Joshua J. White, Antonia De Maio, Kihoon Han,
1038 Ji-Yoen Kim, Paymaan Jafar-Nejad, Alberto di Ronza, Hyojin Kang, Layal S. Sayegh,
1039 Thomas A. Cooper, Harry T. Orr, Roy V. Sillitoe, and Huda Y. Zoghbi. Pumilio1 Haploin-
1040 sufficiency Leads to SCA1-like Neurodegeneration by Increasing Wild-Type Ataxin1 Levels.
1041 *Cell*, 160(6):1087–1098, March 2015. ISSN 0092-8674. doi: 10.1016/j.cell.2015.02.012.

1042 [22] Meng Zhang, Dong Chen, Jing Xia, Wenqi Han, Xiekui Cui, Nils Neuenkirchen, Gretchen
1043 Hermes, Nenad Sestan, and Haifan Lin. Post-transcriptional regulation of mouse neurogenesis
1044 by Pumilio proteins. *Genes & Development*, 31(13):1354–1369, July 2017. ISSN 0890-9369,
1045 1549-5477. doi: 10.1101/gad.298752.117.

1046 [23] Siraj K. Zahr, Guang Yang, Hilal Kazan, Michael J. Borrett, Scott A. Yuzwa, Anastassia
1047 Voronova, David R. Kaplan, and Freda D. Miller. A Translational Repression Complex in
1048 Developing Mammalian Neural Stem Cells that Regulates Neuronal Specification. *Neuron*,
1049 97(3):520–537.e6, February 2018. ISSN 0896-6273. doi: 10.1016/j.neuron.2017.12.045.

1050 [24] Hongxin Dong, Mengyi Zhu, Liping Meng, Yan Ding, Ding Yang, Shanshan Zhang, Wenan
1051 Qiang, Daniel W. Fisher, Eugene Yujun Xu, Hongxin Dong, Mengyi Zhu, Liping Meng, Yan
1052 Ding, Ding Yang, Shanshan Zhang, Wenan Qiang, Daniel W. Fisher, and Eugene Yujun Xu.
1053 Pumilio2 regulates synaptic plasticity via translational repression of synaptic receptors in
1054 mice. *Oncotarget*, 5(0), January 2018. ISSN 1949-2553. doi: 10.18632/oncotarget.24345.

1055 [25] Ryo Narita, Kiyohiro Takahasi, Etsu Murakami, Emi Hirano, Seiji P. Yamamoto, Mitsutoshi
1056 Yoneyama, Hiroki Kato, and Takashi Fujita. A Novel Function of Human Pumilio Proteins
1057 in Cytoplasmic Sensing of Viral Infection. *PLOS Pathogens*, 10(10):e1004417, October 2014.
1058 ISSN 1553-7374. doi: 10.1371/journal.ppat.1004417.

1059 [26] Michèle Brocard, Sarika Khasnis, C. David Wood, Claire Shannon-Lowe, and Michelle J.
1060 West. Pumilio directs deadenylation-associated translational repression of the cyclin-
1061 dependent kinase 1 activator RGC-32. *Nucleic Acids Research*, 46(7):3707–3725, April 2018.
1062 ISSN 0305-1048. doi: 10.1093/nar/gky038.

1063 [27] Martijn Kedde, Marieke van Kouwenhove, Wilbert Zwart, Joachim A. F. Oude Vrielink, Ran
1064 Elkon, and Reuven Agami. A Pumilio-induced RNA structure switch in p27-3' UTR controls
1065 miR-221 and miR-222 accessibility. *Nature Cell Biology*, 12(10):1014–1020, October 2010.
1066 ISSN 1476-4679. doi: 10.1038/ncb2105.

1067 [28] Sungyul Lee, Florian Kopp, Tsung-Cheng Chang, Anupama Sataluri, Beibei Chen, Sushama
1068 Sivakumar, Hongtao Yu, Yang Xie, and Joshua T. Mendell. Noncoding RNA NORAD Reg-
1069 ulates Genomic Stability by Sequestering PUMILIO Proteins. *Cell*, 164(1–2):69–80, January
1070 2016. ISSN 0092-8674. doi: 10.1016/j.cell.2015.12.017.

1071 [29] Cécile Naudin, Aurore Hattabi, Fabio Michelet, Ayda Miri-Nezhad, Aissa Benyoucef,
1072 Françoise Pflumio, François Guillonneau, Serge Fichelson, Isabelle Vigon, Isabelle Dusanter-
1073 Fourt, and Evelyne Lauret. PUMILIO/FOXP1 signaling drives expansion of hematopoietic
1074 stem/progenitor and leukemia cells. *Blood*, 129(18):2493–2506, May 2017. ISSN 0006-4971,
1075 1528-0020. doi: 10.1182/blood-2016-10-747436.

1076 [30] Ailone Tichon, Rotem Ben-Tov Perry, Lovorka Stojic, and Igor Ulitsky. SAM68 is required
1077 for regulation of Pumilio by the NORAD long noncoding RNA. *Genes & Development*, 32
1078 (1):70–78, January 2018. ISSN 0890-9369, 1549-5477. doi: 10.1101/gad.309138.117.

1079 [31] Vincenzo A. Gennarino, Elizabeth E. Palmer, Laura M. McDonell, Li Wang, Carolyn J.
1080 Adamski, Amanda Koire, Lauren See, Chun-An Chen, Christian P. Schaaf, Jill A. Rosenfeld,
1081 Jessica A. Panzer, Ute Moog, Shuang Hao, Ann Bye, Edwin P. Kirk, Pawel Stankiewicz,
1082 Amy M. Breman, Arran McBride, Tejaswi Kandula, Holly A. Dubbs, Rebecca Macintosh,
1083 Michael Cardamone, Ying Zhu, Kevin Ying, Kerith-Rae Dias, Megan T. Cho, Lindsay B.
1084 Henderson, Berivan Baskin, Paula Morris, Jiang Tao, Mark J. Cowley, Marcel E. Dinger, Tony
1085 Roscioli, Oana Caluseriu, Oksana Suchowersky, Rani K. Sachdev, Olivier Lichtarge, Jianrong
1086 Tang, Kym M. Boycott, J. Lloyd Holder, and Huda Y. Zoghbi. A Mild PUM1 Mutation
1087 Is Associated with Adult-Onset Ataxia, whereas Haploinsufficiency Causes Developmental
1088 Delay and Seizures. *Cell*, 172(5):924–936.e11, February 2018. ISSN 00928674. doi: 10.1016/
1089 j.cell.2018.02.006.

1090 [32] Jamie Van Etten, Trista L. Schagat, Joel Hrit, Chase Weidmann, Justin Brumbaugh,
1091 Joshua J. Coon, and Aaron C. Goldstrohm. Human Pumilio proteins recruit multiple
1092 deadenylases to efficiently repress messenger RNAs. *Journal of Biological Chemistry*, page
1093 jbc.M112.373522, September 2012. ISSN 0021-9258, 1083-351X. doi: 10.1074/jbc.M112.
1094 373522.

1095 [33] Chase A. Weidmann, Nathan A. Raynard, Nathan H. Blewett, Jamie Van Etten, and Aaron C.
1096 Goldstrohm. The RNA binding domain of Pumilio antagonizes poly-adenosine binding protein
1097 and accelerates deadenylation. *RNA*, 20(8):1298–1319, January 2014. ISSN 1355-8382, 1469-
1098 9001. doi: 10.1261/rna.046029.114.

1099 [34] Jennifer A. Bohn, Jamie L. Van Etten, Trista L. Schagat, Brittany M. Bowman, Richard C.
1100 McEachin, Peter L. Freddolino, and Aaron C. Goldstrohm. Identification of diverse target
1101 RNAs that are functionally regulated by human Pumilio proteins. *Nucleic Acids Research*,
1102 46(1):362–386, January 2018. ISSN 0305-1048. doi: 10.1093/nar/gkx1120.

1103 [35] Adam R. Morris, Neelanjan Mukherjee, and Jack D. Keene. Ribonomic Analysis of Human
1104 Pum1 Reveals cis-trans Conservation across Species despite Evolution of Diverse mRNA
1105 Target Sets. *Molecular and Cellular Biology*, 28(12):4093–4103, June 2008. ISSN 0270-7306,
1106 1098-5549. doi: 10.1128/MCB.00155-08.

1107 [36] Alessia Galgano, Michael Forrer, Lukasz Jaskiewicz, Alexander Kanitz, Mihaela Zavolan, and
1108 André P. Gerber. Comparative Analysis of mRNA Targets for Human PUF-Family Proteins

1109 Suggests Extensive Interaction with the miRNA Regulatory System. *PLOS ONE*, 3(9):e3164,
1110 September 2008. ISSN 1932-6203. doi: 10.1371/journal.pone.0003164.

1111 [37] Markus Hafner, Markus Landthaler, Lukas Burger, Mohsen Khorshid, Jean Hausser, Philipp
1112 Berninger, Andrea Rothballer, Manuel Ascano, Anna-Carina Jungkamp, Mathias Mun-
1113 schauer, Alexander Ulrich, Greg S. Wardle, Scott Dewell, Mihaela Zavolan, and Thomas
1114 Tuschl. Transcriptome-wide Identification of RNA-Binding Protein and MicroRNA Target
1115 Sites by PAR-CLIP. *Cell*, 141(1):129–141, April 2010. ISSN 00928674. doi: 10.1016/j.cell.
1116 2010.03.009.

1117 [38] Eric L. Van Nostrand, Gabriel A. Pratt, Alexander A. Shishkin, Chelsea Gelboin-Burkhart,
1118 Mark Y. Fang, Balaji Sundararaman, Steven M. Blue, Thai B. Nguyen, Christine Surka,
1119 Keri Elkins, Rebecca Stanton, Frank Rigo, Mitchell Guttman, and Gene W. Yeo. Ro-
1120 bust transcriptome-wide discovery of RNA-binding protein binding sites with enhanced CLIP
1121 (eCLIP). *Nature Methods*, 13(6):508–514, June 2016. ISSN 1548-7091. doi: 10.1038/nmeth.
1122 3810.

1123 [39] Michelle T. Paulsen, Artur Veloso, Jayendra Prasad, Karan Bedi, Emily A. Ljungman, Brian
1124 Magnuson, Thomas E. Wilson, and Mats Ljungman. Use of Bru-Seq and BruChase-Seq for
1125 genome-wide assessment of the synthesis and stability of RNA. *Methods*, 67(1):45–54, May
1126 2014. ISSN 1046-2023. doi: 10.1016/j.ymeth.2013.08.015.

1127 [40] M. Ohtsu, M. Kawate, M. Fukuoka, W. Gunji, F. Hanaoka, T. Utsugi, F. Onoda, and Y. Mu-
1128 rakukani. Novel DNA Microarray System for Analysis of Nascent mRNAs. *DNA Research*, 15
1129 (4):241–251, May 2008. ISSN 1340-2838, 1756-1663. doi: 10.1093/dnares/dsn015.

1130 [41] Edward Yang, Erik van Nimwegen, Mihaela Zavolan, Nikolaus Rajewsky, Mark Schroeder,
1131 Marcelo Magnasco, and James E Darnell Jr. Decay Rates of Human mRNAs: Correlation
1132 With Functional Characteristics and Sequence Attributes. *Genome Research*, page 11, 2003.

1133 [42] L. V. Sharova, A. A. Sharov, T. Nedorezov, Y. Piao, N. Shaik, and M. S.H. Ko. Database
1134 for mRNA Half-Life of 19 977 Genes Obtained by DNA Microarray Analysis of Pluripotent
1135 and Differentiating Mouse Embryonic Stem Cells. *DNA Research*, 16(1):45–58, January 2009.
1136 ISSN 1340-2838, 1756-1663. doi: 10.1093/dnares/dsn030.

1137 [43] Björn Schwankhäusser, Dorothea Busse, Na Li, Gunnar Dittmar, Johannes Schuchhardt, Jana
1138 Wolf, Wei Chen, and Matthias Selbach. Global quantification of mammalian gene expression
1139 control. *Nature*, 473(7347):337–342, May 2011. ISSN 0028-0836, 1476-4687. doi: 10.1038/
1140 nature10098.

1141 [44] ENCODE Project Consortium. An integrated encyclopedia of DNA elements in the hu-
1142 man genome. *Nature*, 489(7414):57–74, September 2012. ISSN 1476-4687. doi: 10.1038/
1143 nature11247.

1144 [45] Stephen G. Landt, Georgi K. Marinov, Anshul Kundaje, Pouya Kheradpour, Florencia Pauli,
1145 Serafim Batzoglou, Bradley E. Bernstein, Peter Bickel, James B. Brown, Philip Cayting,
1146 Yiwen Chen, Gilberto DeSalvo, Charles Epstein, Katherine I. Fisher-Aylor, Ghia Euskirchen,
1147 Mark Gerstein, Jason Gertz, Alexander J. Hartemink, Michael M. Hoffman, Vishwanath R.
1148 Iyer, Youngsook L. Jung, Subhradip Karmakar, Manolis Kellis, Peter V. Kharchenko, Qunhua
1149 Li, Tao Liu, X. Shirley Liu, Lijia Ma, Aleksandar Milosavljevic, Richard M. Myers, Peter J.
1150 Park, Michael J. Pazin, Marc D. Perry, Debasish Raha, Timothy E. Reddy, Joel Rozowsky,

1151 Noam Shoresh, Arend Sidow, Matthew Slattery, John A. Stamatoyannopoulos, Michael Y.
1152 Tolstorukov, Kevin P. White, Simon Xi, Peggy J. Farnham, Jason D. Lieb, Barbara J. Wold,
1153 and Michael Snyder. ChIP-seq guidelines and practices of the ENCODE and modENCODE
1154 consortia. *Genome Research*, 22(9):1813–1831, January 2012. ISSN 1088-9051, 1549-5469.
1155 doi: 10.1101/gr.136184.111.

1156 [46] H. Tani, R. Mizutani, K. A. Salam, K. Tano, K. Ijiri, A. Wakamatsu, T. Isogai, Y. Suzuki,
1157 and N. Akimitsu. Genome-wide determination of RNA stability reveals hundreds of short-
1158 lived noncoding transcripts in mammals. *Genome Research*, 22(5):947–956, May 2012. ISSN
1159 1088-9051. doi: 10.1101/gr.130559.111.

1160 [47] Kenneth Chang, Krista Marran, Amy Valentine, and Gregory J. Hannon. RNAi in Cul-
1161 tured Mammalian Cells Using Synthetic siRNAs. *Cold Spring Harbor Protocols*, 2012(9):
1162 pdb.prot071076, January 2012. ISSN 1940-3402, 1559-6095. doi: 10.1101/pdb.prot071076.

1163 [48] Michael B. Wolfe, Aaron C. Goldstrohm, and Peter L. Freddolino. Global analysis of RNA
1164 metabolism using bio-orthogonal labeling coupled with next-generation RNA sequencing.
1165 *Methods*, December 2018. ISSN 1046-2023. doi: 10.1016/j.ymeth.2018.12.001.

1166 [49] Michael I. Love, Wolfgang Huber, and Simon Anders. Moderated estimation of fold change
1167 and dispersion for RNA-seq data with DESeq2. *Genome Biology*, 15:550, December 2014.
1168 ISSN 1474-760X. doi: 10.1186/s13059-014-0550-8.

1169 [50] Erin L. Sternburg, Jason A. Estep, Daniel K. Nguyen, Yahui Li, and Fedor V. Karginov. An-
1170 tagonistic and cooperative AGO2-PUM interactions in regulating mRNAs. *Scientific Reports*,
1171 8(1):15316, October 2018. ISSN 2045-2322. doi: 10.1038/s41598-018-33596-4.

1172 [51] Daniel Dominguez, Peter Freese, Maria S. Alexis, Amanda Su, Myles Hochman, Tsultrim
1173 Palden, Cassandra Bazile, Nicole J. Lambert, Eric L. Van Nostrand, Gabriel A. Pratt,
1174 Gene W. Yeo, Brenton R. Graveley, and Christopher B. Burge. Sequence, Structure, and
1175 Context Preferences of Human RNA Binding Proteins. *Molecular Cell*, 70(5):854–867.e9,
1176 June 2018. ISSN 1097-2765. doi: 10.1016/j.molcel.2018.05.001.

1177 [52] Inga Jarmoskaite, Sarah K. Denny, Pavanapuresan P. Vaidyanathan, Winston R. Becker,
1178 Johan O. L. Andreasson, Curtis J. Layton, Kalli Kappel, Varun Shivashankar, Raashi Sreeni-
1179 vasan, Rhiju Das, William J. Greenleaf, and Daniel Herschlag. A Quantitative and Predictive
1180 Model for RNA Binding by Human Pumilio Proteins. *Molecular Cell*, May 2019. ISSN 1097-
1181 2765. doi: 10.1016/j.molcel.2019.04.012.

1182 [53] Tzu-Fang Lou, Chase A. Weidmann, Jordan Killingsworth, Traci M. Tanaka Hall, Aaron C.
1183 Goldstrohm, and Zachary T. Campbell. Integrated analysis of RNA-binding protein com-
1184 plexes using in vitro selection and high-throughput sequencing and sequence specificity
1185 landscapes (SEQRS). *Methods*, 118-119:171–181, April 2017. ISSN 10462023. doi:
1186 10.1016/j.ymeth.2016.10.001.

1187 [54] C. Tuerk and L. Gold. Systematic evolution of ligands by exponential enrichment: RNA
1188 ligands to bacteriophage T4 DNA polymerase. *Science*, 249(4968):505–510, August 1990.
1189 ISSN 0036-8075, 1095-9203. doi: 10.1126/science.2200121.

1190 [55] Timothy L. Bailey, Nadya Williams, Chris Misleh, and Wilfred W. Li. MEME: Discovering
1191 and analyzing DNA and protein sequence motifs. *Nucleic Acids Research*, 34(suppl 2):W369–
1192 W373, January 2006. ISSN 0305-1048, 1362-4962. doi: 10.1093/nar/gkl198.

1193 [56] Arttu Jolma, Teemu Kivioja, Jarkko Toivonen, Lu Cheng, Gonghong Wei, Martin Enge,
1194 Mikko Taipale, Juan M. Vaquerizas, Jian Yan, Mikko J. Sillanpää, Martin Bonke, Kimmo
1195 Palin, Shaheynoor Talukder, Timothy R. Hughes, Nicholas M. Luscombe, Esko Ukkonen,
1196 and Jussi Taipale. Multiplexed massively parallel SELEX for characterization of human
1197 transcription factor binding specificities. *Genome Research*, 20(6):861–873, June 2010. ISSN
1198 1088-9051. doi: 10.1101/gr.100552.109.

1199 [57] Arttu Jolma, Jian Yan, Thomas Whitington, Jarkko Toivonen, Kazuhiro R. Nitta, Pasi
1200 Rastas, Ekaterina Morgunova, Martin Enge, Mikko Taipale, Gonghong Wei, Kimmo Palin,
1201 Juan M. Vaquerizas, Renaud Vincentelli, Nicholas M. Luscombe, Timothy R. Hughes, Patrick
1202 Lemaire, Esko Ukkonen, Teemu Kivioja, and Jussi Taipale. DNA-Binding Specificities of
1203 Human Transcription Factors. *Cell*, 152(1-2):327–339, January 2013. ISSN 00928674. doi:
1204 10.1016/j.cell.2012.12.009.

1205 [58] J. Matthew Taliaferro, Nicole J. Lambert, Peter H. Sudmant, Daniel Dominguez, Jason J.
1206 Merkin, Maria S. Alexis, Cassandra A. Bazile, and Christopher B. Burge. RNA Sequence
1207 Context Effects Measured In Vitro Predict In Vivo Protein Binding and Regulation. *Molecular
1208 Cell*, 64(2):294–306, October 2016. ISSN 1097-2765. doi: 10.1016/j.molcel.2016.08.035.

1209 [59] Olivier Elemento, Noam Slonim, and Saeed Tavazoie. A Universal Framework for Regulatory
1210 Element Discovery across All Genomes and Data Types. *Molecular Cell*, 28(2):337–350,
1211 October 2007. ISSN 1097-2765. doi: 10.1016/j.molcel.2007.09.027.

1212 [60] Peng Jiang, Mona Singh, and Hilary A. Coller. Computational assessment of the cooperativity
1213 between RNA binding proteins and MicroRNAs in Transcript Decay. *PLoS computational
1214 biology*, 9(5):e1003075, 2013. ISSN 1553-7358. doi: 10.1371/journal.pcbi.1003075.

1215 [61] Ulrike Brandt-Bohne, Douglas R. Keene, Fletcher A. White, and Manuel Koch. MEGF9:
1216 A novel transmembrane protein with a strong and developmentally regulated expression in
1217 the nervous system. *Biochemical Journal*, 401(2):447–457, January 2007. ISSN 0264-6021,
1218 1470-8728. doi: 10.1042/BJ20060691.

1219 [62] Richard S Jope and Gail V. W Johnson. The glamour and gloom of glycogen synthase
1220 kinase-3. *Trends in Biochemical Sciences*, 29(2):95–102, February 2004. ISSN 0968-0004. doi:
1221 10.1016/j.tibs.2003.12.004.

1222 [63] Olga C. Jorge-Torres, Karolina Szczesna, Laura Roa, Carme Casal, Louisa Gonzalez-
1223 Somermeyer, Marta Soler, Cecilia D. Velasco, Pablo Martínez-San Segundo, Paolo Petazzi,
1224 Mauricio A. Sáez, Raúl Delgado-Morales, Stephane Fourcade, Aurora Pujol, Dori Huertas,
1225 Artur Llobet, Sonia Guil, and Manel Esteller. Inhibition of Gsk3b Reduces NfkB1
1226 Signaling and Rescues Synaptic Activity to Improve the Rett Syndrome Phenotype in
1227 Mecp2 -Knockout Mice. *Cell Reports*, 23(6):1665–1677, May 2018. ISSN 22111247. doi:
1228 10.1016/j.celrep.2018.04.010.

1229 [64] Lindsey N. Kent and Gustavo Leone. The broken cycle: E2F dysfunction in cancer. *Nature
1230 Reviews Cancer*, page 1, May 2019. ISSN 1474-1768. doi: 10.1038/s41568-019-0143-7.

1231 [65] Wayne O. Miles, Katrin Tschöp, Anabel Herr, Jun-Yuan Ji, and Nicholas J. Dyson. Pumilio
1232 facilitates miRNA regulation of the E2F3 oncogene. *Genes & Development*, 26(4):356–368,
1233 February 2012. ISSN 0890-9369. doi: 10.1101/gad.182568.111.

1234 [66] Bo Wang, Shu-hao Hsu, Xinmei Wang, Huban Kutay, Hemant Kumar Bid, Jianhua Yu,
1235 Ramesh K. Ganju, Samson T. Jacob, Mariia Yuneva, and Kalpana Ghoshal. Reciprocal reg-
1236 ulation of microRNA-122 and c-Myc in hepatocellular cancer: Role of E2F1 and transcrip-
1237 tion factor dimerization partner 2: Wang et al. *Hepatology*, 59(2):555–566, February 2014. ISSN
1238 02709139. doi: 10.1002/hep.26712.

1239 [67] Vikram Agarwal, George W Bell, Jin-Wu Nam, and David P Bartel. Predicting effective
1240 microRNA target sites in mammalian mRNAs. *eLife*, 4:e05005, August 2015. ISSN 2050-
1241 084X. doi: 10.7554/eLife.05005.

1242 [68] Svetlana Lebedeva, Marvin Jens, Kathrin Theil, Björn Schwahnhäusser, Matthias Selbach,
1243 Markus Landthaler, and Nikolaus Rajewsky. Transcriptome-wide Analysis of Regulatory
1244 Interactions of the RNA-Binding Protein HuR. *Molecular Cell*, 43(3):340–352, August 2011.
1245 ISSN 1097-2765. doi: 10.1016/j.molcel.2011.06.008.

1246 [69] Jun Wang, Yan Guo, Huili Chu, Yaping Guan, Jingwang Bi, and Baocheng Wang. Multiple
1247 Functions of the RNA-Binding Protein HuR in Cancer Progression, Treatment Responses
1248 and Prognosis. *International Journal of Molecular Sciences*, 14(5):10015–10041, May 2013.
1249 doi: 10.3390/ijms140510015.

1250 [70] Hani Goodarzi, Olivier Elemento, and Saeed Tavazoie. Revealing Global Regulatory Per-
1251 turbations across Human Cancers. *Molecular Cell*, 36(5):900–911, December 2009. ISSN
1252 1097-2765. doi: 10.1016/j.molcel.2009.11.016.

1253 [71] Kelly D. Sullivan, Thomas E. Mullen, William F. Marzluff, and Eric J. Wagner. Knockdown
1254 of SLBP results in nuclear retention of histone mRNA. *RNA*, 15(3):459–472, March 2009.
1255 ISSN 1355-8382. doi: 10.1261/rna.1205409.

1256 [72] Kent L. Rossman, Channing J. Der, and John Sondek. GEF means go: Turning on RHO
1257 GTPases with guanine nucleotide-exchange factors. *Nature Reviews Molecular Cell Biology*,
1258 6(2):167, February 2005. ISSN 1471-0080. doi: 10.1038/nrm1587.

1259 [73] Liyana Ahmad, Shen-Ying Zhang, Jean-Laurent Casanova, and Vanessa Sancho-Shimizu.
1260 Human TBK1: A Gatekeeper of Neuroinflammation. *Trends in molecular medicine*, 22(6):
1261 511–527, June 2016. ISSN 1471-4914. doi: 10.1016/j.molmed.2016.04.006.

1262 [74] Dragana Jankovic, Paolo Gorello, Ting Liu, Sabire Ehret, Roberta La Starza, Cecile
1263 Desjobert, Florent Baty, Martin Brutsche, Padma-Sheila Jayaraman, Alessandra Santoro,
1264 Christina Mecucci, and Juerg Schwaller. Leukemogenic mechanisms and targets of a
1265 NUP98/HHEX fusion in acute myeloid leukemia. *Blood*, 111(12):5672–5682, June 2008. ISSN
1266 0006-4971, 1528-0020. doi: 10.1182/blood-2007-09-108175.

1267 [75] Jian Xu, Vijay G. Sankaran, Min Ni, Tobias F. Menne, Rishi V. Puram, Woojin Kim, and
1268 Stuart H. Orkin. Transcriptional silencing of γ -globin by BCL11A involves long-range inter-
1269 actions and cooperation with SOX6. *Genes & Development*, 24(8):783–798, April 2010. ISSN
1270 0890-9369, 1549-5477. doi: 10.1101/gad.1897310.

1271 [76] Xavier Caubit, Paolo Gubellini, Joris Andrieux, Pierre L. Roubertoux, Mehdi Metwaly,
1272 Bernard Jacq, Ahmed Fatmi, Laurence Had-Aïssouni, Kenneth Y. Kwan, Pascal Salin,
1273 Michèle Carlier, Agne Liedén, Eva Rudd, Marwan Shinawi, Catherine Vincent-Delorme,
1274 Jean-Marie Cuisset, Marie-Pierre Lemaitre, Fatimetou Abderrehamane, Bénédicte Duban,

1275 Jean-François Lemaitre, Adrian S. Woolf, Detlef Bockenhauer, Dany Severac, Emeric Dubois,
1276 Ying Zhu, Nenad Sestan, Alistair N. Garratt, Lydia Kerkerian-Le Goff, and Laurent Fasano.
1277 *TSHZ3* deletion causes an autism syndrome and defects in cortical projection neurons. *Nature*
1278 *Genetics*, 48(11):1359–1369, November 2016. ISSN 1546-1718. doi: 10.1038/ng.3681.

1279 [77] Torsten Hothorn, Kurt Hornik, and Achim Zeileis. Unbiased Recursive Partitioning: A
1280 Conditional Inference Framework. *Journal of Computational and Graphical Statistics*, 15(3):
1281 651–674, September 2006. ISSN 1061-8600. doi: 10.1198/106186006X133933.

1282 [78] Silke Janitz, Carolin Strobl, and Anne-Laure Boulesteix. An AUC-based permutation vari-
1283 able importance measure for random forests. *BMC Bioinformatics*, 14(1):119, December
1284 2013. ISSN 1471-2105. doi: 10.1186/1471-2105-14-119.

1285 [79] Oliver Hobert. Gene Regulation by Transcription Factors and MicroRNAs. *Science*, 319
1286 (5871):1785–1786, March 2008. ISSN 0036-8075, 1095-9203. doi: 10.1126/science.1151651.

1287 [80] Lulu I T. Korsak, Molly E. Mitchell, Katherine A. Shepard, and Michael R. Akins. Regulation
1288 of neuronal gene expression by local axonal translation. *Current genetic medicine reports*, 4
1289 (1):16–25, March 2016. ISSN 2167-4876. doi: 10.1007/s40142-016-0085-2.

1290 [81] Julia A. Kaye, Natalie C. Rose, Brett Goldsworthy, Andrei Goga, and Noelle D. L'Etoile.
1291 A 3'UTR Pumilio-Binding Element Directs Translational Activation in Olfactory Sensory
1292 Neurons. *Neuron*, 61(1):57–70, January 2009. ISSN 0896-6273. doi: 10.1016/j.neuron.2008.
1293 11.012.

1294 [82] Gang Lu and Traci M. Tanaka Hall. Alternate Modes of Cognate RNA Recognition by
1295 Human PUMILIO Proteins. *Structure*, 19(3):361–367, March 2011. ISSN 0969-2126. doi:
1296 10.1016/j.str.2010.12.019.

1297 [83] Anthony M. Mustoe, Steven Busan, Greggory M. Rice, Christine E. Hajdin, Brant K.
1298 Peterson, Vera M. Ruda, Neil Kubica, Razvan Nutiu, Jeremy L. Baryza, and Kevin M.
1299 Weeks. Pervasive Regulatory Functions of mRNA Structure Revealed by High-Resolution
1300 SHAPE Probing. *Cell*, 173(1):181–195.e18, March 2018. ISSN 0092-8674, 1097-4172. doi:
1301 10.1016/j.cell.2018.02.034.

1302 [84] Bastian Linder, Anya V. Grozhik, Anthony O. Olarerin-George, Cem Meydan, Christo-
1303 pher E. Mason, and Samie R. Jaffrey. Single-nucleotide-resolution mapping of m6A and
1304 m6Am throughout the transcriptome. *Nature Methods*, 12(8):767–772, August 2015. ISSN
1305 1548-7105. doi: 10.1038/nmeth.3453.

1306 [85] Megan E. Forrest, Ashrut Narula, Thomas J Sweet, Daniel Arango, Gavin Hanson, James
1307 Ellis, Shalini Oberdoerffer, Jeff Coller, and Olivia S Rissland. Codon usage and amino acid
1308 identity are major determinants of mRNA stability in humans. *bioRxiv*, December 2018. doi:
1309 10.1101/488676.

1310 [86] Gavin Hanson and Jeff Coller. Codon optimality, bias and usage in translation and mRNA
1311 decay. *Nature Reviews Molecular Cell Biology*, 19(1):20–30, January 2018. ISSN 1471-0080.
1312 doi: 10.1038/nrm.2017.91.

1313 [87] Qiushuang Wu, Santiago Gerardo Medina, Gopal Kushawah, Michelle Lynn DeVore, Lu-
1314 ciana A Castellano, Jacqelyn M Hand, Matthew Wright, and Ariel Alejandro Bazzini. Trans-
1315 lation affects mRNA stability in a codon-dependent manner in human cells. *eLife*, 8:e45396,
1316 April 2019. ISSN 2050-084X. doi: 10.7554/eLife.45396.

1317 [88] Vladimir Presnyak, Najwa Alhusaini, Ying-Hsin Chen, Sophie Martin, Nathan Morris,
1318 Nicholas Kline, Sara Olson, David Weinberg, Kristian E. Baker, Brenton R. Graveley, and
1319 Jeff Coller. Codon Optimality Is a Major Determinant of mRNA Stability. *Cell*, 160(6):
1320 1111–1124, March 2015. ISSN 0092-8674. doi: 10.1016/j.cell.2015.02.029.

1321 [89] René M. Arvola, Chase A. Weidmann, Traci M. Tanaka Hall, and Aaron C. Goldstrohm.
1322 Combinatorial control of messenger RNAs by Pumilio, Nanos and Brain Tumor Proteins.
1323 *RNA Biology*, 14(11):1445–1456, November 2017. ISSN 1547-6286. doi: 10.1080/15476286.
1324 2017.1306168.

1325 [90] Ji-Young Youn, Wade H. Dunham, Seo Jung Hong, James D.R. Knight, Mikhail Bashkurov,
1326 Ginny I. Chen, Halil Bagci, Bhavisha Rathod, Graham MacLeod, Simon W.M. Eng, Stéphane
1327 Angers, Quaid Morris, Marc Fabian, Jean-François Côté, and Anne-Claude Gingras. High-
1328 Density Proximity Mapping Reveals the Subcellular Organization of mRNA-Associated Gran-
1329 ules and Bodies. *Molecular Cell*, 69(3):517–532.e11, February 2018. ISSN 10972765. doi:
1330 10.1016/j.molcel.2017.12.020.

1331 [91] Yoav Benjamini and Yosef Hochberg. Controlling the False Discovery Rate: A Practical and
1332 Powerful Approach to Multiple Testing. *J. R. Statist. Soc. B*, 57(1):289–300, 1995.

1333 [92] Timothy L. Bailey, Mikael Boden, Fabian A. Buske, Martin Frith, Charles E. Grant, Luca
1334 Clementi, Jingyuan Ren, Wilfred W. Li, and William S. Noble. MEME Suite: Tools for
1335 motif discovery and searching. *Nucleic Acids Research*, 37(suppl 2):W202–W208, January
1336 2009. ISSN 0305-1048, 1362-4962. doi: 10.1093/nar/gkp335.

1337 [93] Anthony M. Bolger, Marc Lohse, and Bjoern Usadel. Trimmomatic: A flexible trimmer for
1338 Illumina Sequence Data. *Bioinformatics*, page btu170, April 2014. ISSN 1367-4803, 1460-
1339 2059. doi: 10.1093/bioinformatics/btu170.

1340 [94] Marcel Martin. Cutadapt removes adapter sequences from high-throughput sequencing reads.
1341 *EMBnet.journal*, 17(1):pp. 10–12, May 2011. ISSN 2226-6089. doi: 10.14806/ej.17.1.200.

1342 [95] Alexander Dobin, Carrie A. Davis, Felix Schlesinger, Jorg Drenkow, Chris Zaleski, Sonali
1343 Jha, Philippe Batut, Mark Chaisson, and Thomas R. Gingeras. STAR: Ultrafast universal
1344 RNA-seq aligner. *Bioinformatics*, 29(1):15–21, January 2013. ISSN 1367-4803, 1460-2059.
1345 doi: 10.1093/bioinformatics/bts635.

1346 [96] Torsten Hothorn, Peter Bühlmann, Sandrine Dudoit, Annette Molinaro, and Mark J. Van
1347 Der Laan. Survival ensembles. *Biostatistics*, 7(3):355–373, July 2006. ISSN 1465-4644. doi:
1348 10.1093/biostatistics/kxj011.

1349 [97] Carolin Strobl, Anne-Laure Boulesteix, Achim Zeileis, and Torsten Hothorn. Bias in random
1350 forest variable importance measures: Illustrations, sources and a solution. *BMC Bioinfor-
1351 matics*, 8(1):25, December 2007. ISSN 1471-2105. doi: 10.1186/1471-2105-8-25.

1352 [98] Carolin Strobl, Anne-Laure Boulesteix, Thomas Kneib, Thomas Augustin, and Achim Zeileis.
1353 Conditional variable importance for random forests. *BMC Bioinformatics*, 9(1):307, Decem-
1354 ber 2008. ISSN 1471-2105. doi: 10.1186/1471-2105-9-307.

1355 [99] Jesse Davis and Mark Goadrich. The relationship between Precision-Recall and ROC curves.
1356 pages 233–240. ACM Press, 2006. ISBN 978-1-59593-383-6. doi: 10.1145/1143844.1143874.

1357 [100] Debashish Ray, Hilal Kazan, Kate B. Cook, Matthew T. Weirauch, Hamed S. Najafabadi,
1358 Xiao Li, Serge Guerousov, Mihai Albu, Hong Zheng, Ally Yang, Hong Na, Manuel Irimia,
1359 Leah H. Matzat, Ryan K. Dale, Sarah A. Smith, Christopher A. Yarosh, Seth M. Kelly,
1360 Behnam Nabet, Desirea Mecenas, Weimin Li, Rakesh S. Laishram, Mei Qiao, Howard D.
1361 Lipshitz, Fabio Piano, Anita H. Corbett, Russ P. Carstens, Brendan J. Frey, Richard A. An-
1362 derson, Kristen W. Lynch, Luiz O. F. Penalva, Elissa P. Lei, Andrew G. Fraser, Benjamin J.
1363 Blencowe, Quaid D. Morris, and Timothy R. Hughes. A compendium of RNA-binding motifs
1364 for decoding gene regulation. *Nature*, 499(7457):172–177, July 2013. ISSN 0028-0836. doi:
1365 10.1038/nature12311.

1366 [101] Ronny Lorenz, Stephan H. Bernhart, Christian Höner zu Siederdissen, Hakim Tafer,
1367 Christoph Flamm, Peter F. Stadler, and Ivo L. Hofacker. ViennaRNA Package 2.0. *Al-
1368 gorithms for Molecular Biology*, 6:26, 2011. ISSN 1748-7188. doi: 10.1186/1748-7188-6-26.

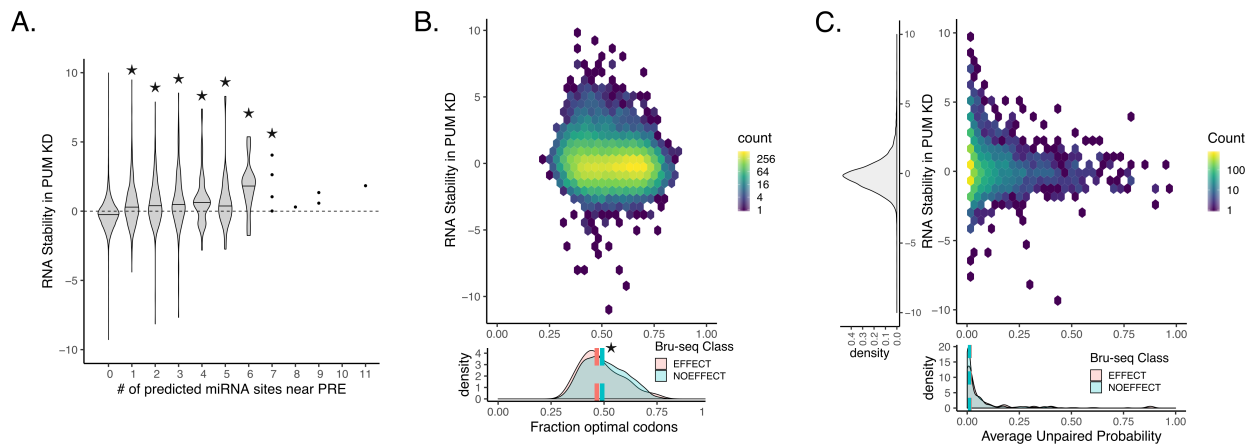
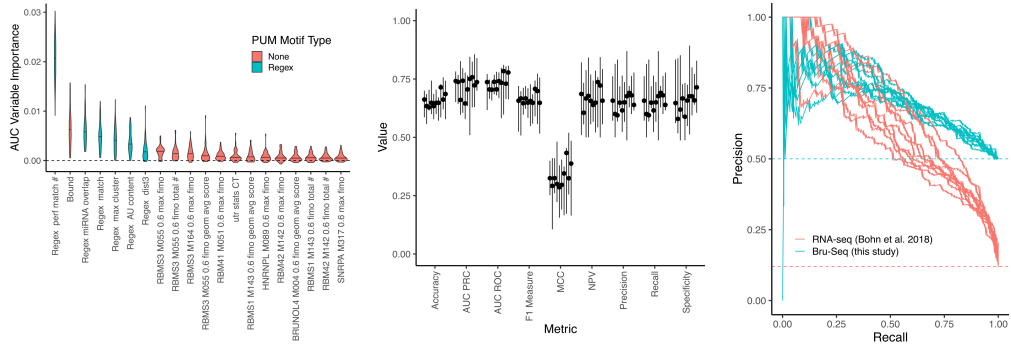
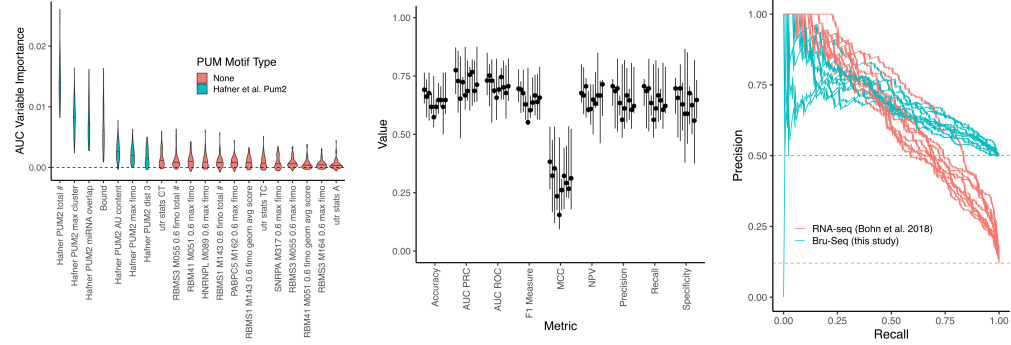


Figure S1: Additional features considered in determining PUM-mediated decay. A) Count of predicted conserved miRNA sites from conserved families that overlapped within 100 bp of a PRE for each gene. Stars indicate statistical significance from a Wilcoxon rank sum test compared to the 0 overlapping miRNA case. Stability in PUM knockdown is represented by a normalized interaction term between time and condition, where positive values indicate stabilization upon PUM knockdown and negative values indicate destabilization upon PUM knockdown (see Methods for details). B) (Above) Relationship between the fraction optimal codons as determined by the Codon Stability Coefficient determined in HEK293 cells [87] and PUM-mediated effect as measured in our Bru-seq data. (Below) Marginal density plots of the fraction optimal codons for genes in the EFFECT and NOEFFECT classes. Median fraction optimal codons for each class are plotted with dotted lines. A significant ($p < 0.05$, two-sided permutation test, $n = 1000$) difference in medians between the classes is indicated by a star. C) (Above) Relationship between the probability of a given PRE being unpaired in predicted RNA secondary structure. Only genes with a PRE with > 0 probability of being unpaired where shown in the heatmap. All other genes are shown in the marginal y-axis density plot. (Below) Marginal density plot for genes in the EFFECT and NOEFFECT classes with median probabilities for each class shown as dotted lines. See Methods for details of secondary structure prediction.

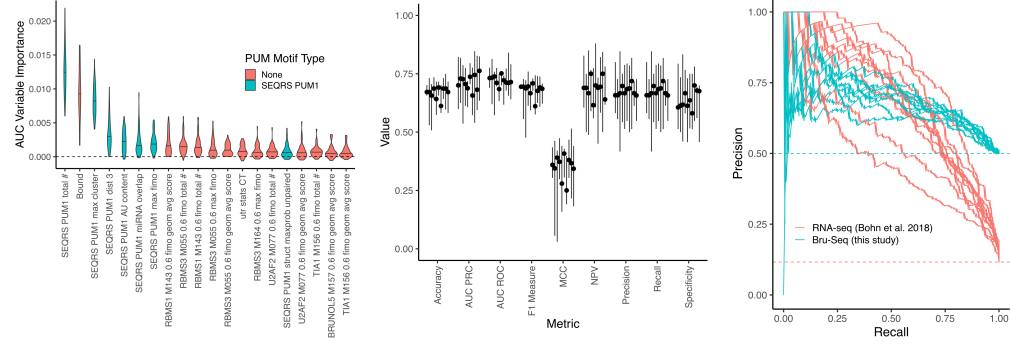
A. Regex



B. Hafner PUM2



C. SEQRS PUM1



D. SEQRS PUM2

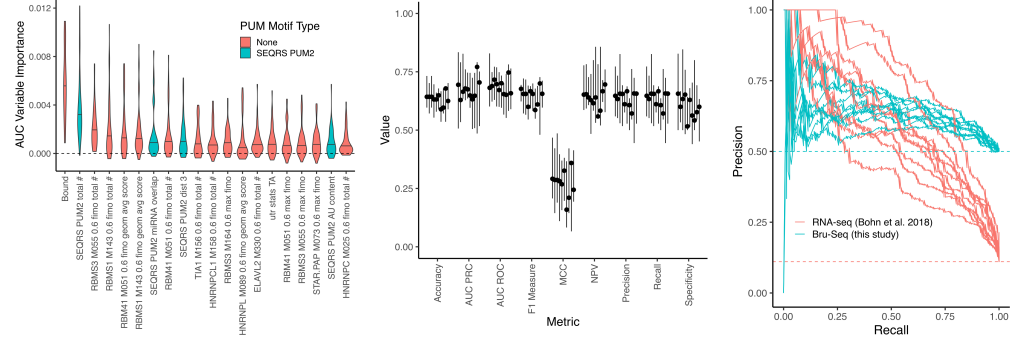


Figure S2 (*previous page*): Predicting PUM-mediated effect subset by motif. A) Conditional random forest models for the datasets considering only genes that had at least one match to the regex motif definition in a 3' UTR. PRE features only consider those around the regex definition. Panels are as in Figure 6B, D, and F. B) As in A), but for the Hafner et al. [37] PUM2 motif. C) As in A), but for the SEQRS PUM1 motif. D) As in A), but for the SEQRS PUM2 motif.